

Published in final edited form as:

Nat Struct Mol Biol. 2020 March ; 27(3): 249–259. doi:10.1038/s41594-020-0384-x.

## A short motif in the N-terminal region of $\alpha$ -synuclein is critical for both aggregation and function

Ciaran P. A. Doherty<sup>1,2</sup>, Sabine M. Ulamec<sup>1,2</sup>, Roberto Maya-Martinez<sup>1</sup>, Sarah C. Good<sup>1</sup>, Jemma Makepeace<sup>1</sup>, G. Nasir Khan<sup>1</sup>, Patricija van Oosten-Hawle<sup>1</sup>, Sheena E. Radford<sup>1,\*</sup>, David J. Brockwell<sup>1,\*</sup>

<sup>1</sup>Astbury Centre for Structural Molecular Biology, School of Molecular and Cellular Biology, Faculty of Biological Sciences, University of Leeds, LS2 9JT, United Kingdom

### Abstract

Aggregation of human  $\alpha$ -synuclein ( $\alpha$ Syn) is linked to Parkinson's disease (PD) pathology. The central region of the  $\alpha$ Syn sequence contains the non-amyloid  $\beta$ -component (NAC) crucial for aggregation. However, how NAC flanking regions modulate  $\alpha$ Syn aggregation remains unclear. Using bioinformatics, mutation, and NMR we identify a 7-residue sequence, named P1 (residues 36-42), that controls  $\alpha$ Syn aggregation. Deletion or substitution of this 'master-controller' prevents aggregation at pH 7.5 *in vitro*. At lower pH, P1 synergises with a sequence containing the PreNAC region (P2, residues 45-57) to prevent aggregation. Deleting P1 ( P1) or both P1 and P2 ( ) also prevents age-dependent  $\alpha$ Syn aggregation and toxicity in *C. elegans* models and prevents  $\alpha$ Syn-mediated vesicle fusion by altering the conformational properties of the protein when lipid-bound. The results highlight the importance of a master-controller sequence motif that controls both  $\alpha$ Syn aggregation and function- a region that could be targeted to prevent aggregation in disease.

---

Users may view, print, copy, and download text and data-mine the content in such documents, for the purposes of academic research, subject always to the full Conditions of use:[http://www.nature.com/authors/editorial\\_policies/license.html#terms](http://www.nature.com/authors/editorial_policies/license.html#terms)

\*Corresponding authors: Sheena E Radford, Tel: +113 343 3170, S.E.Radford@leeds.ac.uk, David J Brockwell, Tel: +113 343 7821; D.J.Brockwell@leeds.ac.uk.

<sup>2</sup>joint first authors

### Data availability

Chemical shift assignments can be accessed using BMRB numbers 27900 (WT- $\alpha$ Syn), 27901 (  $\alpha$ Syn) and 28045 (PIP2-GS  $\alpha$ Syn). Source data for Figure 1c-e, Figure 2a-d, Figure 3a-c, Figure 4a-g, Figure 5a-g, Figure 6b,d, Figure 7a-f and Figure 8d and Extended Figure 1a-h, Extended Figure 2a, Extended Figure 3b-g, Extended Figure 5a,b, Extended Figure 6b,c and Extended Figure 7a-d are available with the paper online. Other datasets generated during and/or analysed during the current study are available in the University of Leeds data repository (<https://doi.org/10.5518/707>).

### Author Contributions

CPAD and SMU prepared samples, designed and performed fluorescence, NMR experiments, EM and other biochemical studies, JM, SCG and PvOH performed the experiments with *C. elegans*. CPAD, SMU and GNK performed CD experiments. RMM performed NMR assignment and assisted with NMR data analysis and interpretation. SER and DJB developed the ideas and supervised the work. All authors contributed to the preparation of the manuscript.

### Competing interests

No authors have competing interests.

## Introduction

The aggregation of  $\alpha$ -synuclein ( $\alpha$ Syn), a neuronal protein with a primary locus at pre-synaptic nerve termini of the central nervous system<sup>1</sup>, is closely associated with Parkinson's disease (PD) and other synucleinopathies<sup>2,3</sup>. PD affects more than 1% of the world population over the age of 60 and 10 million people worldwide<sup>4</sup>. The aetiology of PD and the processes by which  $\alpha$ Syn self-assembles to and causes toxicity is not fully understood. For example, while monomeric  $\alpha$ Syn is intrinsically disordered *in vitro* and *in vivo*<sup>5,6</sup>, it forms an array of oligomers<sup>7,8</sup> and fibril structures<sup>9</sup>, only some of which are cytotoxic or infectious<sup>7</sup>.

The primary sequence of  $\alpha$ Syn comprises three regions (Figure 1A). The N-terminal region (residues 1-60), is basic and contains 6 to 9 conserved imperfect repeats (KTKEGV) crucial for membrane binding<sup>10</sup>. The central NAC region (residues 61-95), has been shown to be necessary and sufficient for the aggregation of  $\alpha$ Syn<sup>11,12</sup>. This region also forms the core of some, but not all,  $\alpha$ Syn amyloid fibril structures<sup>13-15</sup>. Finally, the C-terminal region (residues 96-140) is highly flexible and enriched in acidic residues. Although  $\alpha$ Syn is an intrinsically disordered protein (IDP), it has a smaller radius of gyration<sup>16-18</sup> and collisional cross section<sup>19</sup> than expected for a 140-residue random coil<sup>20</sup>. Its compaction is driven by transient long range electrostatic and hydrophobic interactions between the chemically distinct domains<sup>17,21</sup>. Given its distinct charge patterning (12 basic residues in the N-terminal region and 15 acidic residues in the C-terminal region), the conformational properties of  $\alpha$ Syn are dependent on the solution pH and ionic strength<sup>16-18,21</sup>, which in turn affect the aggregation rate of the NAC region<sup>22,23</sup>.

The effects of sequence changes on the conformational properties and aggregation rates of IDPs have been widely studied<sup>24-28</sup>. Notably for  $\alpha$ Syn, the seven known familial point mutations that lead to early onset PD are clustered in a region (residues 30-53) that flanks NAC (Figure 1A). Deletion of two of the imperfect repeats (residues 9-30), or truncation of the C-terminal region by 11 to 37 residues, increase the rate of  $\alpha$ Syn aggregation<sup>29-31</sup>, while insertion of two additional N-terminal imperfect repeats (by duplication of residues 9-30) inhibits aggregation<sup>30</sup>, highlighting the important, but complex, roles of these regions in modulating assembly. Other studies have suggested that the region preceding NAC (residues 47-56, known as PreNAC) is an important modulator of  $\alpha$ Syn aggregation, as this region contains the familial mutations and is able to aggregate into amyloid-like fibrils in isolation<sup>32</sup>. This sequence also forms the inter-protofilament interface in some<sup>13,14,33</sup>, but not all<sup>13</sup>,  $\alpha$ Syn amyloid fibril structures. However, the molecular mechanism(s) by which this region modulates assembly remain unclear.

Here, we used *in silico* methods to identify two sequence motifs named P1 (residues 36-42) and P2 (residues 45-57) in the N-terminal region of  $\alpha$ Syn that have limited solubility and significant aggregation propensity. We show that these regions are critical for aggregation *in vitro* and when expressed *in vivo* as a  $\alpha$ Syn-YFP fusion in the bodywall muscle cells of *C. elegans*<sup>34</sup>. Paramagnetic relaxation enhancement (PRE) NMR experiments reveal pH- and salt-dependent interactions of these motifs with the NAC and C-terminal regions of the protein, the presence of which correlates with an increased aggregation rate. Finally, we

show that P1 and P2 are important for  $\alpha$ Syn-mediated membrane fusion<sup>35,36</sup>, since their deletion prevents lipid tubule formation and alters the structure of the lipid-bound protein. Together, the results identify P1 as the ‘master-controller’ of  $\alpha$ Syn aggregation as this region governs the conformational properties and aggregation propensity of  $\alpha$ Syn at neutral pH. This region also acts synergistically with P2 (PreNAC) to control assembly at low (lysosomal) pH. The results portray the tug-of-war between function and aggregation in this IDP, with the presence of the P1/P2 regions being essential for vesicle fusion, while simultaneously enhancing amyloid formation.

## Results

### Identification of the P1 and P2 motifs in the N-terminal region of $\alpha$ Syn

To investigate the role of the flanking regions of  $\alpha$ Syn in aggregation we analysed its sequence (Figure 1a) using Zyggregator (amyloid propensity<sup>37</sup>); Camsol (local solubility<sup>38</sup>) and ZipperDB ( $\beta$ -zipper propensity<sup>39</sup>) (Figure 1b-e). This revealed three sequences in the N-terminal region predicted to have low solubility (similar to NAC): <sup>2</sup>DVFMKGL<sup>7</sup>, <sup>36</sup>GVLYVGS<sup>42</sup> (named P1) and <sup>45</sup>KEGVVHGVATVAE<sup>57</sup> (named P2). These regions also have high amyloid propensity as judged by Zyggregator, while ZipperDB identified P2, but not P1 or the N-terminal segment as aggregation-prone. Since the role of the N-terminal region of  $\alpha$ Syn (residues 1-30) has previously been studied by characterisation of deletion<sup>40</sup> and extension<sup>30</sup> variants, this region was not considered further here. The PreNAC region (residues 47-56) was identified by Eisenberg and colleagues<sup>32</sup> and forms part of P2 (residues 45-57). This region also contains six of the seven known familial PD point mutations (Figure 1a). Previous studies have identified a potential role for the P1 and P2 regions in  $\alpha$ Syn aggregation, with 47-56 forming amyloid-like aggregates in isolation<sup>32</sup>, while others have shown that inducing  $\beta$ -hairpin formation in the P1/P2 region (residues <sup>37</sup>VLYVGSK<sup>43</sup> and <sup>48</sup>VVHGVAT<sup>54</sup>) stabilised by binding to a  $\beta$ -wrapin (an engineered binding protein) prevents fibril formation<sup>41-43</sup>. Precisely how these sequences affect aggregation in the intact protein, however, remained unclear.

### The P1 and P2 regions control aggregation

To investigate how P1 and P2 affect  $\alpha$ Syn aggregation, these regions were deleted individually ( P1 and P2) or in tandem ( ) and the rate of aggregation monitored using thioflavin T (ThT) fluorescence and compared with those of WT  $\alpha$ Syn (Figure 2a-d, Extended Data Figure 1a-h and Supplementary Table 1). The aggregates formed after 100 h were also imaged by negative stain transmission electron microscopy (TEM) (Extended Data Figure 1) and fibril yield determined by centrifugation (Supplementary Table 1). The results showed that decreasing the pH from 7.5 to 4.5 (mimicking cytosolic and lysosomal pH, respectively) in 200 mM NaCl accelerates the rate of aggregation of WT  $\alpha$ Syn, decreasing the lag-time ~6-fold and increasing the elongation rate ~10-fold (Figure 2a, Supplementary Table 1) consistent with previous results<sup>44,45</sup>. Aggregation of WT  $\alpha$ Syn is also affected by ionic strength<sup>46</sup>, with assembly into amyloid occurring more rapidly at pH 4.5 at low (20mM added NaCl) compared with high (200 mM added NaCl) ionic strength, while aggregation is more rapid at pH 4.5 than pH 7.5 at both ionic strengths tested (Extended Data Figure 1a,b and Supplementary Table 1).

Remarkably, deleting the 7-residue P1 sequence abolished aggregation (over 100 h) at pH 7.5 at low and high ionic strength (Figure 2b, Extended Data Figure 1d, Supplementary Table 1). Deletion of P1 has a smaller effect at pH 4.5, with little effect at low ionic strength and a ~2-fold increase in the lag time and a ~2-fold decrease in the elongation rate at high ionic strength (Figure 2b, Extended Data Figure 1c, Supplementary Table 1). By contrast, deletion of P2 results in only modest effects under all conditions studied (Figure 2c, Extended Data Figure 1e,f, Supplementary Table 1). Strikingly, the variant did not aggregate (over 100 h) at both pH values at high ionic strength, or at pH 7.5 at low ionic strength, and the lag time of assembly was increased ~15-fold at pH 4.5 in low ionic strength buffer (Figure 2d, Extended Data Figure 1g,h and Supplementary Table 1). This suggests a dominant role for P1 in controlling the aggregation rate of this 140-residue IDP and shows that the effects of P1 are synergistic with P2 at pH 4.5. P1 and were also unable to elongate seeds formed at pH 7.5 from WT  $\alpha$ Syn, whilst P2 formed fibrils slowly (Extended Data Figure 2), suggestive of a structural incompatibility of these sequences with fibril seeds formed from the WT protein.

The importance of P1 and P2 in promoting aggregation was also assessed by measuring the aggregation rate of disulfide cross-linked dimers of  $\alpha$ Syn created by introducing Cys residues in P1 (V40C), P2 (V52C) or at the C-terminus (A140C). In the presence of 2 mM DTT, each variant formed amyloid with kinetics similar to those of WT  $\alpha$ Syn (Figure 3a-c, Supplementary Table 1). Dimerisation (confirmed by SEC-MALS (see Methods)) prevented aggregation (for at least 140 h) for V40C (Figure 3a). However, such an effect was not observed for V52C or A140C (Figure 3b,c, Supplementary Table 1), supporting the finding that P1 is important for aggregation. The positional sensitivity of the dimerisation site was not observed previously when  $\alpha$ Syn was cross-linked by dityrosine formation at Y39 and Y125, Y133 or Y136<sup>47</sup> suggesting a strict steric/positional sensitivity of inhibition. This could act at the stage of dimer formation, or by the imposed dimerisation altering the structure of seeds/oligomers formed later during assembly.

The presence of up to nine imperfect repetitive KTKEGV sequences in the N-terminal region of  $\alpha$ Syn raised the possibility that the effects of deleting P1 and/or P2 may result from changes in the spatial organisation of the repeats (Figure 1b). To assess this possibility, a variant was constructed in which a seven-residue sequence in a different location in the N-terminal region was deleted (residues 14-20, denoted C1) (Figure 1b). C1 was designed to mimic the general features of P1 as closely as possible i.e. the sequence deleted is of the same length and similar positioning between imperfect repeats as P1. In contrast to the marked effects of deleting P1, C1 had no significant effect at pH 7.5 or pH 4.5 at high ionic strength, and even accelerated aggregation (decreasing the lag-time ~10-fold) at pH 4.5 at low ionic strength (Extended Data Figure 3a-d, Supplementary Table 1). Fibrils were also observed after 140 hours in all conditions as judged by negative stain EM and quantification of soluble protein remaining (Extended Data Figure 3g, Supplementary Table 1). A second control variant, named P1P2-GS, was also created in which the 7 residues in P1 and 13 residues in P2 were replaced with alternating Gly-Ser sequences, 7 and 13 residues in length, respectively, preserving the spacing of the imperfect repeats (Extended Data Figure 3a). At pH 7.5 P1P2-GS did not aggregate at low or high ionic strength, similar to the behaviour of (Extended Data Figure 3g,i, Supplementary Table 1). At pH 4.5,

aggregation did occur (Extended Data Figure 3f,i, but was significantly retarded compared with WT  $\alpha$ Syn (Supplementary Table 1). These data show that the effect of P1 and P2 on aggregation is mainly sequence-specific and does not result from alterations in the length of the N-terminal region or the spacing of the imperfect repeats.

### **P1 and P2 make multiple intra-molecular contacts that promote amyloid formation**

To determine whether P1 and P2 affect the conformational properties of  $\alpha$ Syn monomers that alter their ability to assemble into amyloid, WT  $\alpha$ Syn and were examined using Paramagnetic Relaxation Enhancement NMR (PRE NMR). This approach allows rare (0.5 – 5 % population) and transient interactions to be investigated. Previous studies used NMR PREs to investigate the conformational properties of WT  $\alpha$ Syn at pH 2.5, 3.0, 6.0, 7.4 and 7.5 using protein concentrations from 100  $\mu$ M to 650  $\mu$ M at 15  $^{\circ}$ C<sup>17,21,44,48–50</sup>. The familial PD mutations (A30P, A53T)<sup>51</sup> and  $\beta$ - and  $\gamma$ -Syn<sup>52</sup> have also been investigated using this approach. To determine how deletion of P1 and P2 affects the conformational properties of  $\alpha$ Syn monomers, <sup>15</sup>N WT  $\alpha$ Syn containing a single Cys introduced at positions 18 ( $\alpha$ Syn A18C), 90 ( $\alpha$ Syn A90C), or 140 ( $\alpha$ Syn A140C) were expressed, purified and their <sup>1</sup>H-<sup>15</sup>N HSQC spectra assigned at pH 4.5 (Methods). Each protein was then covalently labelled with the paramagnetic spin label S-(1-oxy-2,2,5,5-tetramethyl-2,5-dihydro-1H-pyrrol-3-yl)methyl methanesulfonylthioate (MTSL) and NMR PRE experiments performed to detect transient intramolecular interactions. Control experiments confirmed that inter-molecular interactions are not observed at the protein concentration used (see Methods). Under conditions that promote rapid aggregation of WT  $\alpha$ Syn (pH 4.5, 20 mM NaCl (low salt), Figure 4a) long range intramolecular interactions between specific regions are observed for all three PRE probes (Figure 4b,d,f, Extended Data Figure 4). Specific intramolecular interactions between the N- and C-terminal regions of the protein were observed, as exemplified by significant PRE effects when MTSL was placed at residue 18 (Figure 4b), with a smaller reciprocal PRE effect from MTSL at residue 140 with the N-terminal region (Figure 4f), consistent with previous results at other pH values<sup>17,23,44</sup>. Significant contacts are also observed between NAC and the C-terminal region, consistent with previous analyses at pH 2.5 and 3.0<sup>21,44</sup>. Importantly, and by contrast with previous results<sup>23</sup>, significant PREs are observed between P1 (and some residues in P2) and residues near the N-terminus (using  $\alpha$ Syn A18, Figure 4b), as well as to NAC (using  $\alpha$ Syn A90C, Figure 4d) and to C-terminal regions (using  $\alpha$ Syn A140C, Figure 4f). Previous meta-analysis of 11 PRE NMR studies also showed evidence of the P1 and P2 regions as an interaction hub<sup>53</sup>. Importantly, under conditions in which aggregation is slowed (pH 4.5, 200 mM NaCl (high salt)) (Figure 4a), these intramolecular interactions to P1/P2 (most markedly those involving PREs from residues 90 and 140) are decreased in magnitude (compare Figure 4b,d,f with Figure 4c,e,g), consistent with electrostatic interactions, possibly involving K45, E46, H49 or E57 in P2, or residues that juxtapose P1 (K32, K34, E35, K43) and/or P2 (E61), being involved. The observation that weaker long range intra-molecular interactions with P1/P2 results in slower aggregation kinetics suggests that these interactions are important in defining the aggregation rate.

To determine how removing P1 and P2 affects the conformational properties of monomeric  $\alpha$ Syn, the PRE experiments were repeated under identical conditions (pH 4.5 at low and

high ionic strength) using  $\alpha$ Syn. These conditions result in slow (low salt) or no (high salt) fibril formation, respectively (Figure 5a). The resulting PRE profiles (Figure 5b-g) show that the long range contacts between the N- and C-terminal regions and the NAC and C-terminal region are mostly maintained in  $\alpha$ Syn, while contacts to P1/P2 were removed. Interestingly, while contacts between the N-terminal region (residue 18) and NAC/C-terminal region and NAC (residue 90) and the N-/C-terminal regions are similar in WT and  $\alpha$ Syn, those between the C-terminal region (residue 140) and the N-terminal region are smaller in  $\alpha$ Syn, indicative of a complex interplay of interactions that depends intimately on the sequence and solution conditions. A further control experiment in which intramolecular PREs were measured for P1P2-GS with MTSL at residue 90 showed a similar response, with the long range intra-molecular PREs remaining in this construct and hints that the PRE effect to the P1 and P2 regions observed for WT  $\alpha$ Syn, is significantly reduced in P1P2-GS (Extended Data Figure 5). Thus, removal of P1/P2 does not prevent compaction of the  $\alpha$ Syn sequence, yet a significant reduction in aggregation is observed, demonstrating the crucial importance of the P1/P2 sequences in determining the aggregation of  $\alpha$ Syn.

### The roles of P1 and P2 in initiating intermolecular interactions

At high protein concentrations (500  $\mu$ M),  $\alpha$ Syn forms transient inter-molecular interactions, in which residues 38-45 (corresponding closely to the P1 region (36-42)), make weak inter-chain interactions with residues 124-140, at least at pH 6.0 at low ionic strength (10 mM MES, 0 M NaCl)<sup>54</sup>. To determine whether removal of P1 and P2 disrupts these inter-molecular interactions, 250  $\mu$ M <sup>14</sup>N  $\alpha$ Syn was labelled with MTSL at residue 40 (V40C) or 129 (S129C) and incubated with 250  $\mu$ M <sup>15</sup>N WT  $\alpha$ Syn at pH 4.5 at low and high ionic strength. Intermolecular PREs (via R<sub>2</sub> relaxation experiments) were then measured to identify inter-chain contacts (Extended Data Figure 6a,b). The results showed that residue 40 (in the P1 region) makes intermolecular contacts primarily with residues in the negatively charged C-terminal region of WT  $\alpha$ Syn (Extended Data Figure 6b), in agreement with published results<sup>54</sup>. At high ionic strength (retarded aggregation), this effect is decreased, consistent with these inter-molecular interactions being important in the early stages of aggregation (Extended Data Figure 6b). Finally, intermolecular PREs were determined with MTSL at residue 129 (Extended Data Figure 6c). These experiments showed a significant PRE from residue 129 to the P1 and P2 regions, as well as to the N-terminal ~20 residues in WT  $\alpha$ Syn. Importantly, the latter interactions are maintained in  $\alpha$ Syn, whilst interactions with P1/P2 are no longer possible (Extended Data Figure 6c), showing that the inter-molecular contacts between the N- and C-termini are independent of the presence of P1/P2. Together, the results reinforce the importance of the P1/P2 regions in driving aggregation, not just because of their local insolubility and high aggregation-propensity, but also because they determine the conformational properties of the monomeric IDP and formation of transient intermolecular interactions with the C-terminal region, that define its ability to aggregate into amyloid.

### P1 and P2 are drivers of aggregation *in vivo*

The effect of deleting P1 and P2 on  $\alpha$ Syn aggregation *in vivo* was assessed by expressing WT  $\alpha$ Syn, P1 or P2 fused C-terminally to YFP in *C. elegans* muscle cells<sup>34</sup>. Figure 6a shows that WT  $\alpha$ Syn::YFP forms inclusions that are visible as foci in L4 larvae (Day 0).



Foci increase in number as the animals age, and the proteostasis network declines<sup>55,56</sup>, reaching a plateau from Day 3 to Day 13 of adulthood, as reported previously<sup>34</sup>. In marked contrast, animals expressing P1::YFP or P2::YFP formed few, if any, visible aggregates throughout ageing (Figure 6a,b), even though the expression levels of these proteins is higher than WT  $\alpha$ Syn (Figure 6c). Notably, by contrast with WT  $\alpha$ Syn::YFP, the total number of P1::YFP or P2::YFP foci did not increase during ageing, with few aggregates observed even at Day 13 (Figure 6b). The percentage of immobile WT  $\alpha$ Syn::YFP aggregates increased ~4-fold from Day 7 to Day 13 of adulthood as measured by FRAP (Figure 6b). By comparison, P1 and P2  $\alpha$ Syn::YFP formed only few aggregates (1 to 2 foci) that were immobile (Figure 6b). Even in aged worms motility remained similar to healthy N2 wild-type animals between Days 0-3 (Figure 6d), with slightly reduced (2-fold) thrashing rates observed in P2::YFP and P1::YFP at Day 13 of adulthood (Figure 6d). In contrast, *C. elegans* expressing WT  $\alpha$ Syn::YFP showed an age-dependent decline of motility between Days 3 and 13 compared with N2 worms (Figure 6d). Thus, deletion of P1 or both P1/P2 prevents both age-dependent aggregation of  $\alpha$ Syn *in vivo* and suppresses aggregation-induced proteotoxicity.

### The importance of P1/P2 in membrane remodelling

As P1 and P2 are located in the membrane-binding N-terminal region of  $\alpha$ Syn, we explored whether P1/P2 also play a role in the function of  $\alpha$ Syn in remodelling membrane vesicles<sup>35,57,58</sup>.  $\alpha$ Syn forms  $\alpha$ -helical structure in its N-terminal region (residues 1-97) upon membrane binding<sup>59,60</sup> which subsequently enhances aggregation of the protein into amyloid fibrils<sup>61</sup>. To determine whether P1/P2 is also able to adopt  $\alpha$ -helical structure upon lipid binding, and whether this induces fibril formation, the protein was incubated with liposomes prepared from 1,2-dimyristoyl-sn-glycero-3-phospho-L-serine (DMPS), one of the major lipids in synaptic vesicles. The secondary structure of the protein was then monitored using far UV CD. The resulting data (Figure 7a,b and Extended Data Figure 7a) showed that P1/P2 is able to bind to these vesicles, but adopts only 30% helical structure when membrane bound, whilst 64 % helicity would be expected assuming similar helix formation to WT  $\alpha$ Syn. Lipid titration experiments revealed that the affinity of P1/P2 for lipid is ~10-fold weaker than WT  $\alpha$ Syn ( $K_D = 2.01 \pm 0.63 \mu\text{M}$  and  $0.22 \pm 0.13 \mu\text{M}$  for P1/P2 and WT  $\alpha$ Syn, respectively) (Figure 7a,b, Extended Data Figure 7b). The stoichiometry value, L, indicative of the total number of DMPS molecules in the bilayer involved in binding one  $\alpha$ Syn molecule, is similar for both proteins (49 and 33, respectively) (Figure 7a,b, Extended Data Figure 7b). P1P2-GS responds to DMPS liposomes similarly to P1/P2 (Figure 7c, Extended Data Figure 7b,c). Thus, the effect of P1/P2 is sequence specific and does not result from changing the spacing of the imperfect repeats.

DMPS liposomes have also been shown to accelerate  $\alpha$ Syn aggregation by promoting heterogeneous primary nucleation<sup>61</sup>. To assess whether P1/P2  $\alpha$ Syn is able to nucleate amyloid formation when bound to these 160 nm diameter liposomes (Extended Data Figure 7d), the aggregation kinetics of WT  $\alpha$ Syn, P1/P2 and P1P2-GS were monitored at different [DMPS]: [ $\alpha$ Syn] molar ratios (Figure 7d-f). Consistent with previous results, WT  $\alpha$ Syn does not form amyloid in the absence of liposomes under the conditions employed (20 mM sodium phosphate, pH 6.5)<sup>61</sup>, while an excess of lipid (60:1 [M:M]) also prevents aggregation by

depleting the concentration of lipid-free monomer available for elongation<sup>61</sup>. At an 8:1 [DMPS]:[ $\alpha$ Syn] ratio, however, WT  $\alpha$ Syn aggregates rapidly (Figure 7d), as reported previously<sup>61</sup>. While  $\alpha$ Syn is able to nucleate amyloid formation at a ratio of 8:1 [M:M] [DMPS]:[ $\alpha$ Syn], the rate of aggregation is slowed significantly (lag times =  $4.9 \pm 0.3$  h and  $93.0 \pm 2.6$  h for WT and  $\alpha$ Syn<sup>E46K</sup>, respectively) (Figure 7e, Supplementary Table 1), presumably because less helical structure is formed in  $\alpha$ Syn in the lipid-bound state. Consistent with this P1P2-GS is able to aggregate, but very slowly, when lipid bound (Figure 7c,f and Extended Data Figure 7b). Negative stain TEM of sample at the endpoints of these incubations at 60:1 [DMPS]:[ $\alpha$ Syn] [M:M] are shown in (Figures 7g-i). Remarkably, while WT  $\alpha$ Syn causes the coalescence of liposomes into long lipid tubes, as reported previously<sup>35</sup>, this is not observed upon incubation with  $\alpha$ Syn<sup>E46K</sup> or P1P2-GS. Instead, incubation with these proteins results in the formation of small, prefibrillar-like aggregates (Figure 7h,i (inset)) which associate with the liposome surfaces and appear to cause liposome fission, releasing smaller spherical liposomes (Figure 7h,i). Thus, in addition to controlling the aggregation of  $\alpha$ Syn *in vitro* and *in vivo*, P1/P2 affect the function of  $\alpha$ Syn in re-modelling lipid vesicles.

Finally, membrane binding of WT,  $\alpha$ Syn<sup>E46K</sup> and P1P2-GS were measured in residue-specific detail by acquiring <sup>15</sup>N-<sup>1</sup>H HSQC NMR spectra of the proteins in the presence or absence of saturating amounts (60:1 {M:M} [DMPS]:[ $\alpha$ Syn]) of liposomes (Figure 8a-c). Due to the slow tumbling rates of liposomes, resonances of residues that bind strongly are reduced in intensity, whilst those of lipid free/weakly bound residues have higher intensity in the liposome-bound state<sup>62</sup>. Strikingly, these data showed significant differences in the residues involved in lipid binding, with all but the C-terminal ~20 residues binding strongly to lipid in  $\alpha$ Syn<sup>E46K</sup>, whilst a much smaller interface is formed for WT  $\alpha$ Syn. P1P2-GS exhibited intermediate behaviour, suggesting that both the sequence and the relative position of P1 and P2 play a role in lipid binding (Figure 8d). Thus, the P1/P2-regions control the lipid-binding properties of distal regions of the  $\alpha$ Syn sequence, structure in the lipid-bound state and perturb membrane remodelling, without preventing binding to DMPS liposomes.

## Discussion

### The P1 sequence is a ‘master-controller’ of $\alpha$ Syn aggregation

We have identified a sequence in the N-terminal region of  $\alpha$ Syn (residues 36-42 (P1)) that plays a key role in determining the ability of the protein to form amyloid fibrils *in vitro* and *in vivo*. Remarkably, we show that the seven residue P1 segment is specifically required for aggregation, with its deletion preventing aggregation *in vitro* at neutral pH and in bodywall muscle cells of *C. elegans*, despite the protein retaining the crucial NAC region<sup>12</sup>. By performing aggregation assays and NMR PRE experiments under conditions which either favour (pH 4.5 (lysosomal conditions), low ionic strength) or deter (pH 7.5 (cytosolic), high ionic strength) (Supplementary Table 1) amyloid growth, we have been able to correlate changes in monomer conformation (e.g. changes in the intra-molecular long-range interactions for P1/P2 measured by NMR-PRE at pH 4.5) induced by sequence changes in the P1/P2 region with aggregation propensity. Based on these observations we define the P1 region as a ‘master-controller’ of  $\alpha$ Syn aggregation, in that this region controls  $\alpha$ Syn self-assembly, synergistically with the P2 (Pre-NAC) region<sup>32</sup> under some conditions



(specifically at low pH values that mimic the lysosomal environment, relevant for  $\alpha$ Syn *in vivo*<sup>63</sup>). These regions exert their control by fine-tuning intra- and inter-molecular contacts both locally within the N-terminal region, and with the distal NAC and C-terminal regions, yielding a conformational ensemble that is either aggregation-prone (retaining P1 or P1/P2) or protected from aggregation (P1 or P1/P2 deleted or substituted with Gly-Ser), presumably via exposure/sequestration of the crucial<sup>12,22,23</sup> NAC region. The precise molecular mechanism by which this is accomplished, including the relative importance of each residue in P1 in defining the protein's behaviour, remain to be elucidated. Deletion of P1/P2 could also affect the structure and aggregation-competence of oligomers formed later during aggregation. Whatever the precise mechanism of action, the sensitivity of aggregation to pH and ionic strength suggests that P1/P2 control  $\alpha$ Syn aggregation by a delicate balance of hydrophobicity and charge, such that aggregation becomes highly sensitive to the solution conditions. This may rationalise why P1/P2 interactions eluded detection in previous studies at pH values below<sup>21,44,48</sup> or above<sup>17,44,48-50</sup> pH 4.5. Thus, while NAC is necessary and sufficient for  $\alpha$ Syn aggregation<sup>12</sup>, the ability to prevent aggregation at pH 7.5 by removal or substitution of a single, specific, 7-residue sequence provides a striking demonstration of the crucial effect of flanking regions in amyloid formation.

The importance of flanking region(s) has been demonstrated for other aggregation-prone proteins, including the P17 region in exon 1 of huntingtin<sup>25,26,28</sup>, the N-terminal region (residue 11-16) of amyloid  $\beta$  ( $A\beta_{40}$ )<sup>64</sup>, residues 306-311 in tau<sup>65</sup>, the aggregation prone motifs 14-22, 53-58, and 69-72 in the N-terminal region of Apo-I<sup>24</sup> and the N-terminal six amino acids of  $\beta_2$ -microglobulin<sup>66</sup>. At longer timescales, or under more favourable conditions for aggregation (e.g. at pH 4.5 and low ionic strength (Extended Data Figure 1g) or at pH 6.5 in the presence of DMPS liposomes (Figure 7e)), is able to form amyloid, highlighting the crucial role of the transient intra- and inter-molecular interactions made by the N-terminal region of  $\alpha$ Syn in imposing kinetic control on the thermodynamically favourable process of amyloid formation.

Our discovery that P1 and P2 are also required for the function of  $\alpha$ Syn in vesicle remodelling adds to the growing evidence that the N-terminal region of  $\alpha$ Syn is important for both its physiological function and its disease aetiology<sup>57,67</sup>. Notably, P2 encompasses six of the seven early onset familial PD mutations<sup>68</sup> (Figure 1b). This region also forms the protofilament interface in some<sup>13,14,33</sup>, but not all<sup>13</sup>, structures of  $\alpha$ Syn fibrils formed *in vitro*, and this region can form amyloid in isolation<sup>32</sup>. Hoyer and colleagues also showed that the aggregation of  $\alpha$ Syn can be inhibited *in vitro* and *in vivo* by the binding of a  $\beta$ -wrapin<sup>41,43</sup> to residues 37-54, which encompasses both P1 and P2, with the NMR structure of the complex revealing  $\beta$ -hairpin formation involving residues <sup>37</sup>VLYVGSK<sup>43</sup> and <sup>48</sup>VHGVAT<sup>54</sup> of  $\alpha$ Syn<sup>41</sup>. Engineering an intramolecular disulphide bond between residues 41 and 48 has also been shown to inhibit  $\alpha$ Syn aggregation in the absence of  $\beta$ -hairpin formation<sup>42</sup>, presumably because this perturbs the structure around P1 and P2 that we show here to be vital for fibril formation. Mutation of Y39 to Ala also prevents aggregation and Y39 has been shown to be responsible (together with F94) for binding small molecules able to retard aggregation<sup>62</sup>. Finally, a cyclised peptide of residue 36-55 has been shown to adopt a  $\beta$ -hairpin structure that self-assembles into cytotoxic oligomers, the authors suggesting that this region, rather than NAC, nucleates oligomer formation<sup>11</sup>. Together, the data

presented here highlight the vital importance of P1 and P2 in controlling  $\alpha$ Syn aggregation, demonstrating that aggregation is not initiated by the NAC region alone. Using a *C. elegans* model expressing  $\alpha$ Syn in the bodywall muscles, deletion of P1 or both P1 and P2 suppressed age-dependent  $\alpha$ Syn inclusion body formation as well as the associated toxicity, resulting in animals with improved health-span, even at advanced age. Displacing the interactions made by P1 and/or P2 may thus pave the way to routes to control  $\alpha$ Syn aggregation using small molecules or other reagents that target these sites.

### Frustration between aggregation and function

Given that deletion of P1 and P2 neutralises the deleterious effects of NAC on  $\alpha$ Syn aggregation, why is the sequence of these regions retained by evolution? While the physiological function(s) of  $\alpha$ Syn remain unclear, stabilisation, sequestration, and fusion of pre-synaptic vesicles are thought to be involved in its repertoire of functions<sup>36,57,69</sup>. Distinct membrane binding sites within the N-terminal region involving residues 1-25 and 65-97 have been proposed to play a critical role in tethering vesicles prior to membrane fusion<sup>35,36</sup>. Here we show that deleting part of the ‘passive’ linker region between these two sites (residues 36-57 in P1/P2) prevents the function of  $\alpha$ Syn in membrane remodelling, generating liposome morphologies that are distinct from the large fused tubular structures formed by the WT protein (Figure 7g-i). Together with their effects on aggregation, the results demonstrate the frustration between function and aggregation in this IDP, with the presence of the P1/P2 region being required for function, whilst simultaneously generating a sequence that enhances amyloid assembly. Such a delicate balance rationalises why single point mutations such as A53T, E46K and others<sup>68</sup>, enhance Parkinson’s disease onset by simultaneously causing loss-of-function and gain-of-toxic function activities. For an IDP such as  $\alpha$ Syn the aggregation propensity of such aggregation-prone, yet functionally important regions, cannot be protected by the framework of a folded tertiary structure, making such sequences especially prone to be the causative agents of disease. Indeed 17 of the 48 currently known human amyloidogenic proteins are IDPs or contain intrinsically disordered regions<sup>3</sup>. Such sequences enable dangerous liaisons since their intrinsic amyloid potential is exposed, unabridged by the protection of a native structure. Nonetheless, the presence of such newly discovered and characterised ‘master-controllers’ of aggregation within the  $\alpha$ Syn sequence offers exciting potentials to control amyloid formation by binding small molecules, chaperones, biologics or other agents to these regions. Given the fine balance of weak intra- and inter-molecular interactions that control the early stages of aggregation into amyloid, minor alterations in the shape of the interaction energy landscape could disable aggregation without significantly perturbing function. Further experiments will be needed to identify whether other IDPs contain ‘master-controllers’ of aggregation, to identify the role of each of the seven amino acids in P1 in encoding the ability to control  $\alpha$ Syn aggregation and function and to clarify the molecular mechanism of fibril growth inhibition by P1 in more detail.

## Methods

### Mutagenesis, expression and purification

$\alpha$ Syn containing single Cys variants, the P1P2-GS control (P1 (7 aa) replaced with (SG)<sub>3</sub>S and P2 (13 aa) with (GS)<sub>6</sub>G) and/or deletions of C1, P1 and/or the P2 regions were engineered into the gene sequence for WT  $\alpha$ Syn via Q5 site directed mutagenesis (NEB). <sup>14</sup>N, <sup>15</sup>N and <sup>13</sup>C/<sup>15</sup>N labelled  $\alpha$ Syn variants were expressed recombinantly in *Escherichia coli* BL21 (DE3) cells and the protein purified as described previously<sup>70</sup>. In the case of <sup>15</sup>N and/or <sup>13</sup>C labelled protein, expression was performed in HCDM1 minimal medium with <sup>15</sup>N enriched NH<sub>4</sub>Cl and <sup>13</sup>C enriched glucose. Note that by contrast with Masuda *et al.*<sup>71</sup> there was no evidence of mis-incorporation of Cys for Try at residue 136, as the correct molecular masses of all proteins were confirmed by mass spectrometry (WT: 14 459 ± 0.27 Da; P1: 13 784 ± 0.50 Da; P2: 13 182 ± 0.96 Da; : 12506 ± 0.03 Da; C1: 13 861 ± 0.56 Da; P1P2-GS: 13947.4 ± 0.06 Da) (spectra are available at <https://doi.org/10.5518/707>). Additionally, the NMR spectrum of all proteins was fully assigned with residue 136 being confirmed as Tyr. Proteins were lyophilised and stored at -20°C. Proteins were resolubilised in buffer immediately before experiments were carried out. There was no evidence for covalent dimers forming during storage (samples were analysed before and after storage by ESI-MS). Different buffer conditions were used to analyse the behaviour of the proteins at pH 7.5 (20mM Tris HCl) or pH 4.5 (20 mM sodium acetate), with high (200 mM NaCl) or low (20 mM NaCl) salt concentrations. The isoelectric points of the protein variants are: WT: 4.67; P1: 4.67; P2: 4.60; : 4.60; C1: 4.72; P1P2-GS: 4.60 (calculated using ProtParam tool from ExPASy).

### *In silico* methods to determine aggregation propensity

The aggregation propensity was analysed by using the online tools Camsol<sup>38</sup>, Zyggregator<sup>37</sup> and ZipperDB<sup>39</sup> at pH 7.0.

### Aggregation assays monitored by ThT fluorescence

100  $\mu$ L samples of 100  $\mu$ M  $\alpha$ Syn variants in the required buffers were incubated with 20  $\mu$ M ThT in sealed 96-well flat bottom assay plates (Corning, non-binding surface) in a FLUOstar Omega plate reader (BMG Labtech) at 37 °C with continuous orbital agitation at 600 rpm. The fluorescence of ThT was excited at 444 nm and fluorescence emission was monitored at 480 nm. The elongation rate was determined by fitting a gradient to the linear part of the ThT-curve, the lag time was taken as the intercept of the line to the baseline fluorescence signal, using OriginPro software (OriginPro 2018b 64Bit). This analysis was performed with a minimum of three replicate experiments. The standard deviations were calculated for repeated measurements (Supplementary Table 1). Fibril yields were determined via centrifugation (30 min 13,000 rpm (Microfuge SN 100/90) and analysis of remaining soluble material compared to the starting material using SDS PAGE. For this, SDS-PAGE gels were imaged on the Alliance Q9 Imager (Uvitec) and band intensities were determined using ImageJ 1.52a. Repeat experiments and loading controls indicating an error of ~10% in quantifying band intensity using this approach. Experiments monitoring lipid-induced aggregation were performed as above, except that aggregation was followed under quiescent conditions, 30 °C with a protein concentration of 50  $\mu$ M. To prepare seeds of WT

$\alpha$ Syn, 500  $\mu$ L of 600  $\mu$ M  $\alpha$ Syn in Tris HCl pH 7.5, 20 mM NaCl was stirred with a magnet stirrer at 1200 rpm at 45 °C for 48 h. Fibrils were then sonicated twice for 30 sec with a break of 30 sec at 40 % maximum power using a Cole-Parmer-Ultraprocessor-Sonicator. The resulting seeds (10 % (v/v)) were added to 100  $\mu$ M monomer and elongation measured in 20 mM Tris HCl, pH 7.5, containing 20 mM NaCl, 20  $\mu$ M ThT at 37 °C using quiescent conditions.

### Negative stain TEM

Samples at ThT incubation endpoints (usually 100 h) were diluted 1 in 10 or 1 in 5 with 18 M $\Omega$  H<sub>2</sub>O and then applied to carbon coated copper grids in a dropwise fashion. Grids were then dried with filter paper, washed three times with 18 M $\Omega$  H<sub>2</sub>O in a dropwise fashion, drying with filter paper after each wash, before fibril samples were negatively stained by the addition of 1% (w/v) uranyl acetate, added and blotted twice as before. Images were recorded on a Joel JEM-1400 or FEI Tecnai T12 electron microscope.

### Preparation of disulfide locked dimeric $\alpha$ Syn species

To allow the formation of disulfide linkages between monomeric  $\alpha$ Syn Cys variants, 400  $\mu$ M  $\alpha$ Syn was incubated in 100 mM, Tris HCl, pH 8.4 for 2 h at room temperature. Protein samples were then added to a HiLoad<sup>TM</sup> 26/60 Superdex 75 preparative grade gel filtration column (GE Healthcare) in 50 mM ammonium bicarbonate, pH 8.0, which allowed monomer and dimers to be resolved. Disulfide locked dimeric  $\alpha$ Syn was then lyophilised and stored at -20 °C. The presence of disulfide linkages was validated using reducing and non-reducing SDS-PAGE with SEC-MALS used to validate the purification of dimeric constructs. For the latter, 50  $\mu$ L of a 30  $\mu$ M sample of  $\alpha$ Syn was injected onto a TOSOH G200SWXL column equilibrated with 20 mM Tris HCl, containing 200 mM NaCl, pH 7.5. The protein peak was eluted into a Wyatt miniDawnTreo system with three angle detection and the data analysed using Astra 6.0.3<sup>®</sup> software supplied with the instrument.

### NMR Backbone assignments of WT $\alpha$ Syn, $\alpha$ Syn P1P2-GS and $\alpha$ Syn

WT and  $\alpha$ Syn variants were <sup>13</sup>C/<sup>15</sup>N uniformly labelled for NMR backbone assignments purposes. 200  $\mu$ M of protein in 20 mM sodium acetate, 20mM NaCl, 10% (v/v) D<sub>2</sub>O, 0.02% (w/v) sodium azide, pH 4.5 at 15 °C was used to acquire triple correlation experiments: HNCO, HNcaCO, HNCACB, HNcoCACB, HNN-TOCSY, hNcaNNH and hNcaNNH. All experiments were acquired using non-uniform sampling, where just 45% of sparse data was recorded on a Bruker AVANCE III 750 MHz spectrometer equipped with a triple resonance TCI-cryoprobe.

NMR data processing and spectra reconstruction were performed using NMRpipe<sup>72</sup> and data analysis with ccpNMR-Analysis software<sup>73</sup>. HN, C <sub>$\alpha$</sub>  and C <sub>$\beta$</sub>  chemical shifts were deposited at Biological Magnetic Resonance Bank (BMRB) with access numbers 27900, 27901 and 28045 for WT  $\alpha$ Syn, and P1P2-GS, respectively.

### Paramagnetic Relaxation Enhancement NMR experiments

$\alpha$ Syn Cys variants were incubated with 5 mM DTT in 20 mM Tris HCl, 200 mM NaCl, pH 7.5 for 30 min. DTT was then removed by a Zeba spin column (PD10 column, GE

Healthcare) and the sample labelled immediately by incubation with a 40-fold molar excess MTSL for 16 h at 4 °C in 20 mM Tris HCl, 200 mM NaCl, pH 7.5. Excess spin label was removed by Zeba spin column (PD10 column) and protein eluted in the required buffer. Spin-labelled  $\alpha$ Syn constructs were used directly or stored at -80 °C. In all cases 100 % labelling at a single site was confirmed using ESI-MS. For intramolecular PRE experiments,  $^1\text{H}$ - $^{15}\text{N}$  HSQC spectra were obtained using 100  $\mu\text{M}$   $^{15}\text{N}$  spin labelled  $\alpha$ Syn in 20 mM acetate buffer pH 4.5 containing 20 mM or 200 mM NaCl, 10% (v/v)  $\text{D}_2\text{O}$ , 0.02% (w/v) sodium azide on an AVANCE III Bruker spectrometer (600 MHz) equipped with a triple channel QCI-P cryoprobe. All NMR experiments were carried out at 15 °C. Diamagnetic spectra were obtained following the addition of 2 mM ascorbic acid. Note that small changes in chemical shift occur upon adding this acid to the protein spectra and reduction was not complete, leading to small residual intensity of some resonances in the spectra especially when MTSL was added to A90C (see legend to Extended Data Figure 4). Note that this does not affect the conclusions drawn since it underestimates, rather than overestimates the magnitude of the PRE measured. Spectra were processed in Topspin (Bruker) using CCPN<sup>74</sup>. Peak heights were used to calculate intensity ratios (paramagnetic/diamagnetic). Control experiments in which 50  $\mu\text{M}$   $^{15}\text{N}$   $\alpha$ Syn and  $^{14}\text{N}$   $\alpha$ Syn-MTSL were mixed showed no PREs, ruling out intermolecular interactions at this protein concentration under the conditions used. PRE effects arising from non-specific binding of the hydrophobic probe MTSL to  $\alpha$ Syn was ruled out by performing experiments in which 100  $\mu\text{M}$  free MTSL was added to 100  $\mu\text{M}$   $^{15}\text{N}$   $\alpha$ Syn WT (lacking Cys) in which no PREs were observed. Replicate measurements of the PRE intensity ratios ( $I/I_0$ ) using different preparations of WT  $\alpha$ Syn in high and low salt conditions enabled per-residue errors to be determined. On average these were  $\pm 0.05$ . These data are available in (<https://doi.org/10.5518/707>). Intermolecular PRE experiments were carried out by mixing 250  $\mu\text{M}$   $^{15}\text{N}$  WT or  $\alpha$ Syn with 250  $\mu\text{M}$   $^{14}\text{N}$ -MTSL labelled protein.  $T_2$  transverse relaxation experiment was performed based in HSQC pulse sequence<sup>75</sup> with 10  $T_2$  delays (from 16.96 to 610.56 ms), under paramagnetic and diamagnetic conditions. Data processing was performed using NMRpipe<sup>72</sup>. Cross peaks intensities at each  $T_2$ -delay were analysed using PINT and fitted to a single exponential decay using PINT. The effective  $\text{H}_\text{N}$ - $\Gamma_2$  rate was calculated as the difference between the  $R_2$  rate in the paramagnetic versus the diamagnetic samples (Equation 1):

$$\Gamma = R_{2, para} - R_{2, dia} \quad \text{Eq. 1}$$

### Maintenance and generation of transgenic *C. elegans* strains and *in vivo* aggregation measurements

The WT  $\alpha$ Syn gene used was fused C-terminally to YFP in vector pPD30.38<sup>34</sup>. This vector was modified to delete amino acids 36-42 ( P1) or residues 36-42 and 45-57 ( ) by PCR mutagenesis. Transgenic *C. elegans* expressing each construct were then generated by microinjection of P1 $\alpha$ Syn::YFP or  $\alpha$ Syn::YFP constructs into the germline of N2 nematodes, resulting in strains PVH214 *pccEx021[unc-54p::a-synuclein P1::YFP]* and PVH198 *pccEx001[unc-54p::a-synuclein P1 P2::YFP]* (Nemamatrix). Nematodes expressing WT $\alpha$ syn::YFP were created using gene bombardment and kindly provided by Ellen Nollen<sup>34</sup>.



For imaging, *C. elegans* was cultured on NGM plates seeded with *E. coli* OP50-1 at 20 °C as described previously<sup>76</sup>. *C. elegans* was imaged using a Zeiss LSM880 confocal fluorescent microscope through a 10× 1.0 or a 20× 1.0 numerical aperture objective with a 514 nm line for excitation of YFP. Before imaging, age-synchronised animals at different ages (Day 0 (L4 stage) to Day 13) were anaesthetised using 5 mM Levamisole solution in M9 buffer and mounted on 2% (w/v) agar pads. The number of  $\alpha$ Syn::YFP foci were then counted and the mobility of all foci in at least 10 animals per time point and in three independent cultures of *C. elegans* (biological replicates) was determined using FRAP, as described previously<sup>34</sup>. Note that the higher expression levels of the P1 and constructs does not affect the FRAP analysis, as FRAP measures relative fluorescence intensities of similar size photo-bleached and unbleached regions within the same animal.

To determine motility of the worms, a total of 30 age-synchronised animals were used for each assay and each experiment was repeated at least three times. Animals were moved into M9 buffer at indicated time points (Day 0 through to Day 13 of adulthood) and thrashing rates were measured by counting body bends for 15 s using the wrMTrck plugin for ImageJ (available at <http://www.phage.dk/plugins/wrmtrck.html>)<sup>77</sup>. Error bars represent SEM of three biological replicates.

### Immunoblotting

Nematodes were collected from plates, washed in M9 buffer, and resuspended in lysis buffer (20 mM Tris HCl, pH 7.5; 10 mM  $\beta$ -mercaptoethanol; 0.5% (v/v) Triton X-100; supplemented with complete protease inhibitor (Roche) before shock freezing in liquid nitrogen. Three freeze-thaw cycles were performed before the worm pellet was ground with a motorized pestle, and lysed on ice, in the presence of 0.025 U/mL benzonase (Sigma). The lysate was centrifuged at 1000 rpm for 1 min in a table top centrifuge to pellet the carcasses. Protein concentration was determined using Bradford assay (Bio-Rad). Samples were then mixed 1:1 with SDS loading buffer (2% (w/v) SDS, 10% (v/v) glycerol, 0.1% (w/v) bromophenol blue, 100 mM DTT), boiled for 10 min and 25  $\mu$ g final protein was loaded onto a 4-20% gradient Tris HCl gel (Bio-Rad). Protein bands were blotted onto a PVDF membrane and  $\alpha$ Syn and tubulin (control) were visualised using a mouse anti- $\alpha$ Syn antibody (syn211 (1:5000) (NeoMarkers)) or mouse anti-tubulin antibody (1:5000) (Sigma), followed by an anti-mouse horse-radish peroxidase-coupled secondary antibody (1:5000). Bands were visualised using the SuperSignal West Pico Plus Chemiluminescence Substrate (Thermo).

### Liposome preparation

1,2-dimyristoyl-sn-glycero-3-phospho-L-serine (DMPS) (sodium salt, Avanti Polar Lipids) was dissolved in 20 mM sodium phosphate buffer, pH 6.5 and stirred at 45 °C for 2 h. The solution was then frozen and thawed 5-times using dry ice and a water bath at 45 °C, respectively. Preparation of liposomes was then carried out by sonication in a bath sonicator (U50 ultrasonic bath, Ultrawave) for 1 h. The sizes of liposomes were measured using dynamic light scattering (DLS). For DLS 250  $\mu$ L of 100  $\mu$ M samples were injected into a Wyatt miniDawnTreos system (equipped with an additional DLS detector) and the data analysed using Astra 6.0.3<sup>®</sup> software supplied with the instrument. Filtered (0.22  $\mu$ m) and

de-gassed buffer, kept cool on ice to minimise bubble formation inside the instrument, was used to obtain 5 min baselines before and after sample injection. A 3 min sample window was used for the analysis by the software. Using this analysis the liposomes were found to have a diameter  $\approx 160$  nm.

### CD spectroscopy and lipid binding experiments

CD samples were prepared by incubating 25  $\mu$ M WT  $\alpha$ Syn, or P1P2-GS with different concentrations of DMPS liposomes in 20 mM sodium phosphate buffer, pH 6.5. Far-UV CD spectra were acquired in 1 mm path length quartz cuvettes (Hellma) using a Chirascan<sup>TM</sup> plus CD Spectrometer (Applied Photophysics). CD spectra were acquired using a 2 nm bandwidth, 1 s time step, data collected at 1 nm increments at 30 °C. An average of 3 scans (190-260 nm) were acquired per sample. The data were fitted to determine the secondary structure content using Dichroweb<sup>78</sup>.

$K_D$  and stoichiometry values were calculated from CD data using the protocol described in<sup>61</sup> using the fitting function shown in Equation 2:

$$x_B = \frac{\left( \left( [\alpha\text{Syn}] + \frac{[\text{DMPS}]}{L} + K_D \right) - \sqrt{\left( \left( [\alpha\text{Syn}] + \frac{[\text{DMPS}]}{L} + K_D \right)^2 - \frac{4[\text{DMPS}][\alpha\text{Syn}]}{L} \right)} \right)}{2[\alpha\text{Syn}]} \quad \text{Eq. 2}$$

where  $x_B$  is the fraction of  $\alpha$ Syn bound to the membrane, L represents the number of DMPS molecules interacting with one molecule of  $\alpha$ -Syn and can be described as:

$$[\text{DMPS}] = L([\text{DMPS}_L] + [B(\text{DMPS}_L)]) \quad \text{Eq. 3}$$

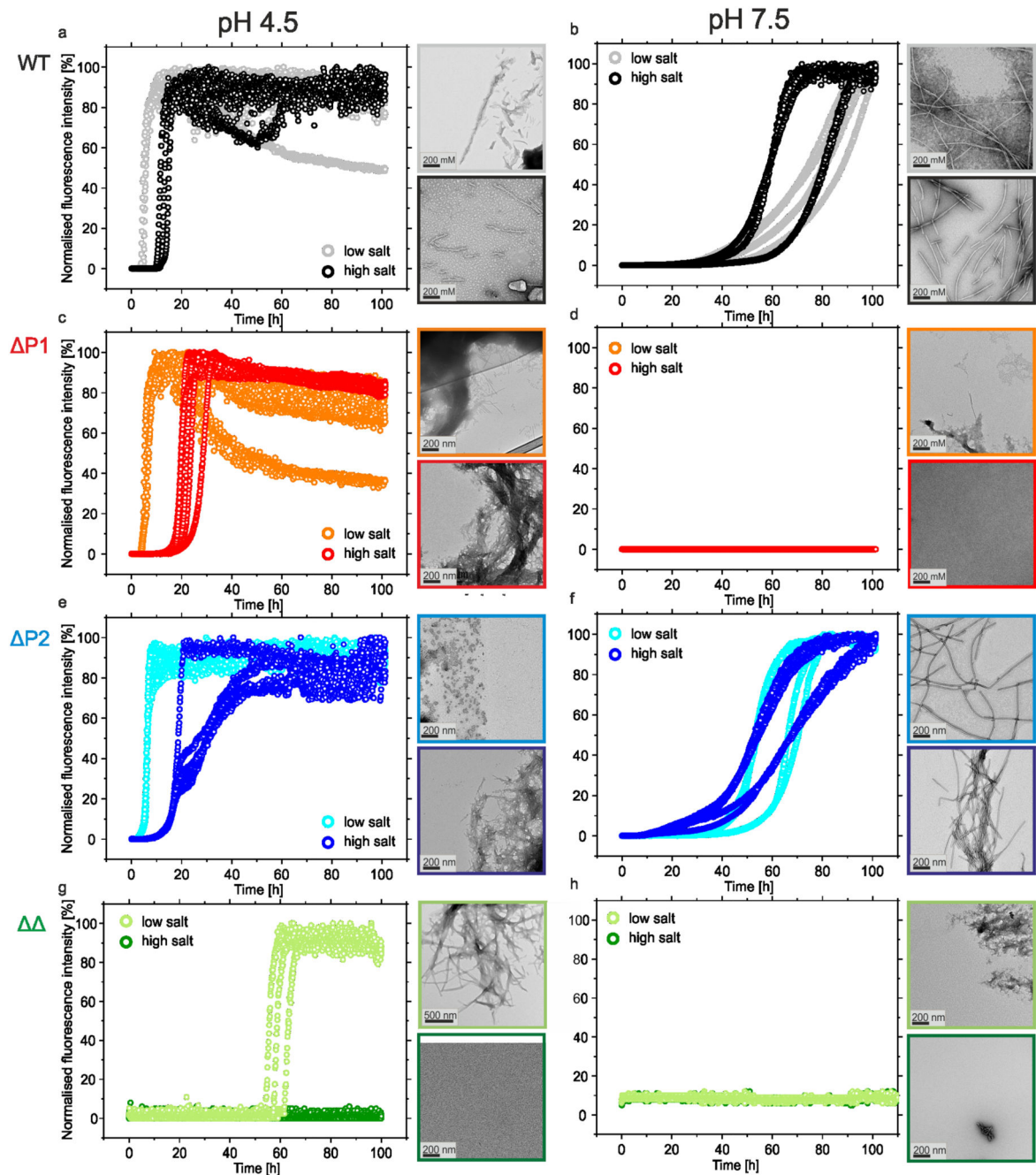
where B is the amount of  $\alpha$ Syn bound to liposomes and L is the number of DMPS molecules interacting with one molecule of  $\alpha$ -Syn.

### NMR experiments to monitor liposome binding

<sup>1</sup>H-<sup>15</sup>N HSQC NMR spectra were obtained using 25  $\mu$ M <sup>15</sup>N WT  $\alpha$ Syn, P1P2-GS or  $\alpha$ Syn in the absence or presence of 60:1 [DMPS]:[ $\alpha$ Syn] ratios. Experiments were carried out in 20 mM sodium phosphate, pH 6.5 (as in<sup>61</sup>) containing 10% (v/v) D<sub>2</sub>O, 0.02% (w/v) sodium azide on an AVANCE III Bruker spectrometer (600 MHz) equipped with a cryogenic probe. All NMR experiments were carried out at 20 °C. Published assignments were used to analyse the data (BMRB 16543)<sup>58</sup>. Spectra were processed in Topspin (Bruker) and analysed in CCPN. Peak heights were used to calculate intensity ratios of  $\alpha$ Syn in the presence versus in the absence of liposomes.

Further information on experimental design is available in the Nature Research Reporting Summary linked to this article

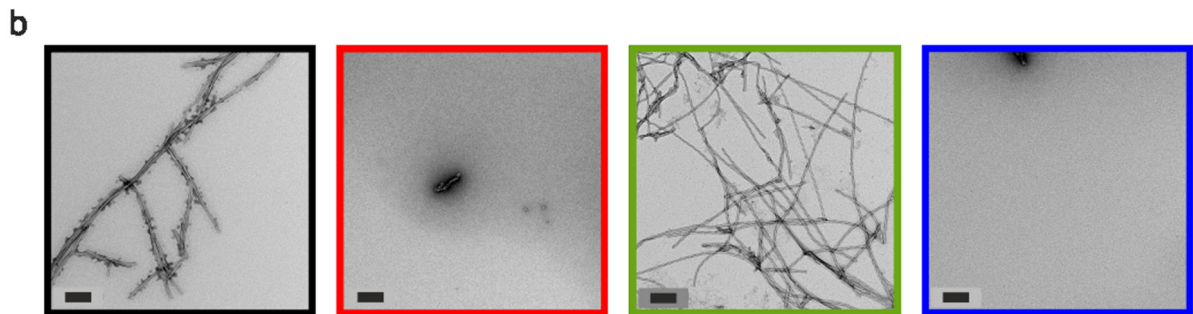
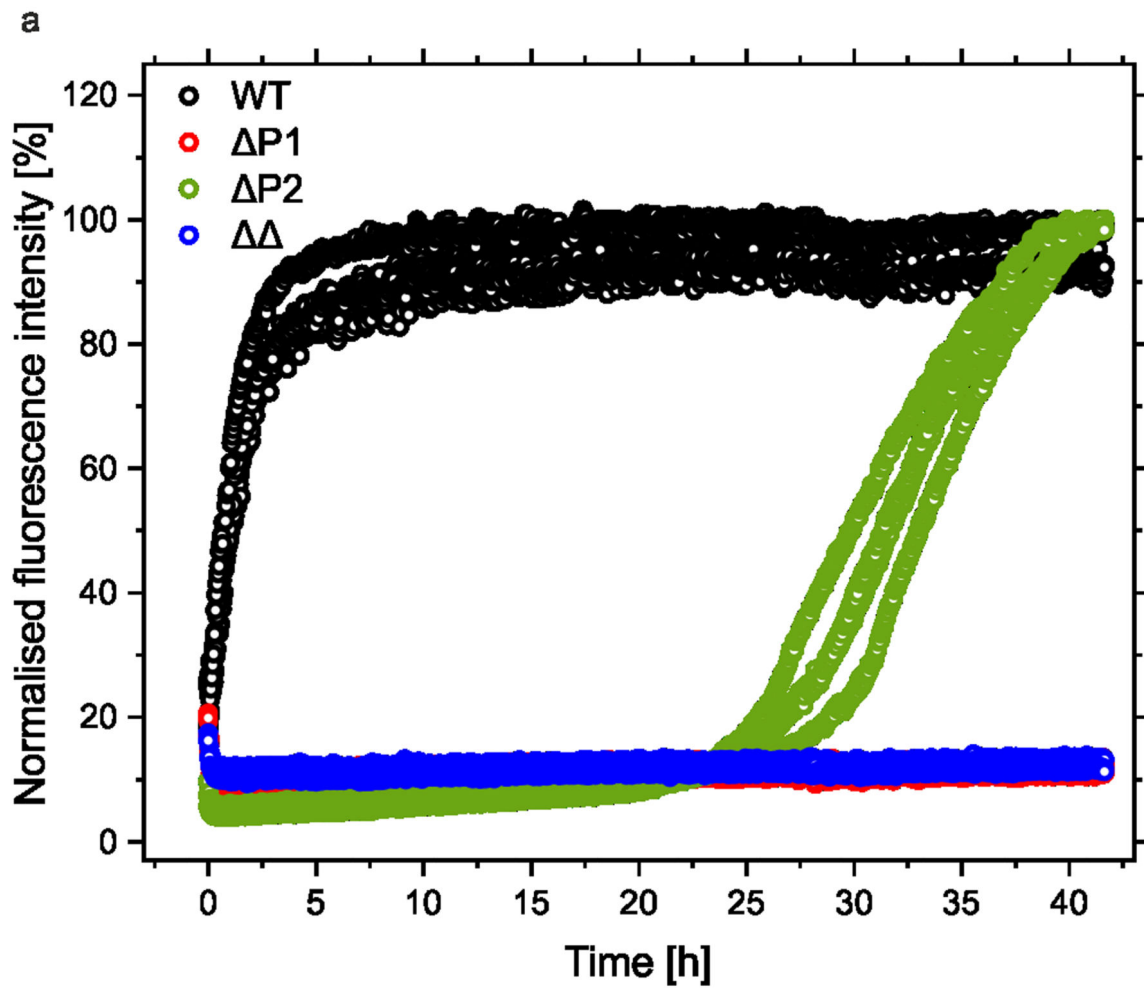
### Extended Data



**Extended data Figure 1. Aggregation kinetics of  $\alpha$ Syn variants at different pH and salt conditions including TEM images of the aggregates (if any) formed at the end point.**

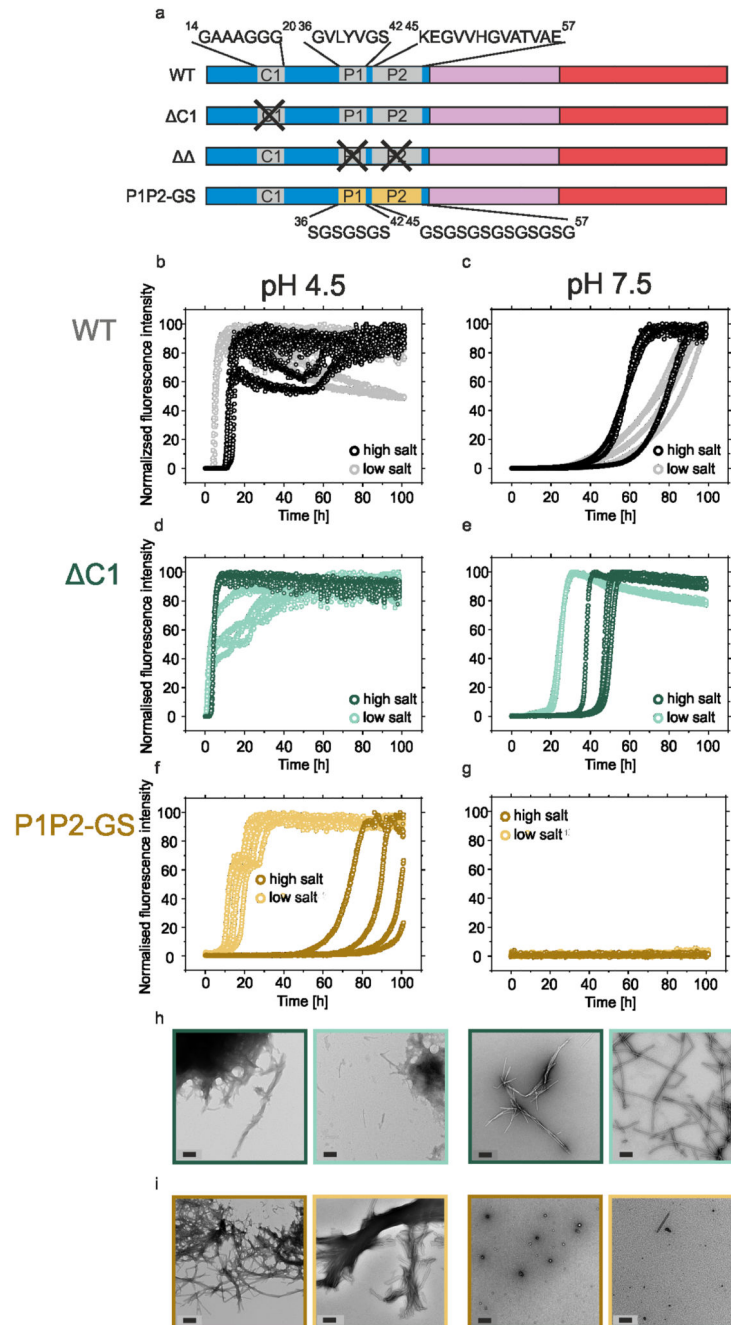
ThT fluorescence assays at pH 4.5 or pH 7.5 of a,b) WT  $\alpha$ Syn, c,d) P1, e,f) P2 and g,h)

at high (200 mM NaCl) or low (20 mM NaCl) ionic strength ( $n = 3$ ). Negative stain TEM images of representative samples of the aggregates formed at the end point (100 h) are shown alongside each plot using the same colour scheme. The fibril yield under each condition, determined by SDS PAGE subsequent to centrifugation (see Methods) is shown in Supplementary Table S1.



**Extended data Figure 2. Cross-seeding  $\alpha$ Syn variants using seeds created from WT  $\alpha$ Syn.**

a) ThT fluorescence assays of  $\alpha$ Syn variants (100  $\mu$ M) WT (black), P1 (red), P2 (green), (blue) seeded with 10 % (v/v) WT  $\alpha$ Syn fibril seeds formed at pH 7.5 (n 3). Seeding assays were performed at pH 7.5, low salt (20 mM added NaCl), 37  $^{\circ}$ C, quiescent. b) End-point (42 h) TEM images of representative samples of fibrils from the seeding experiments using the same colour codes. Scale bars are 200 nm.

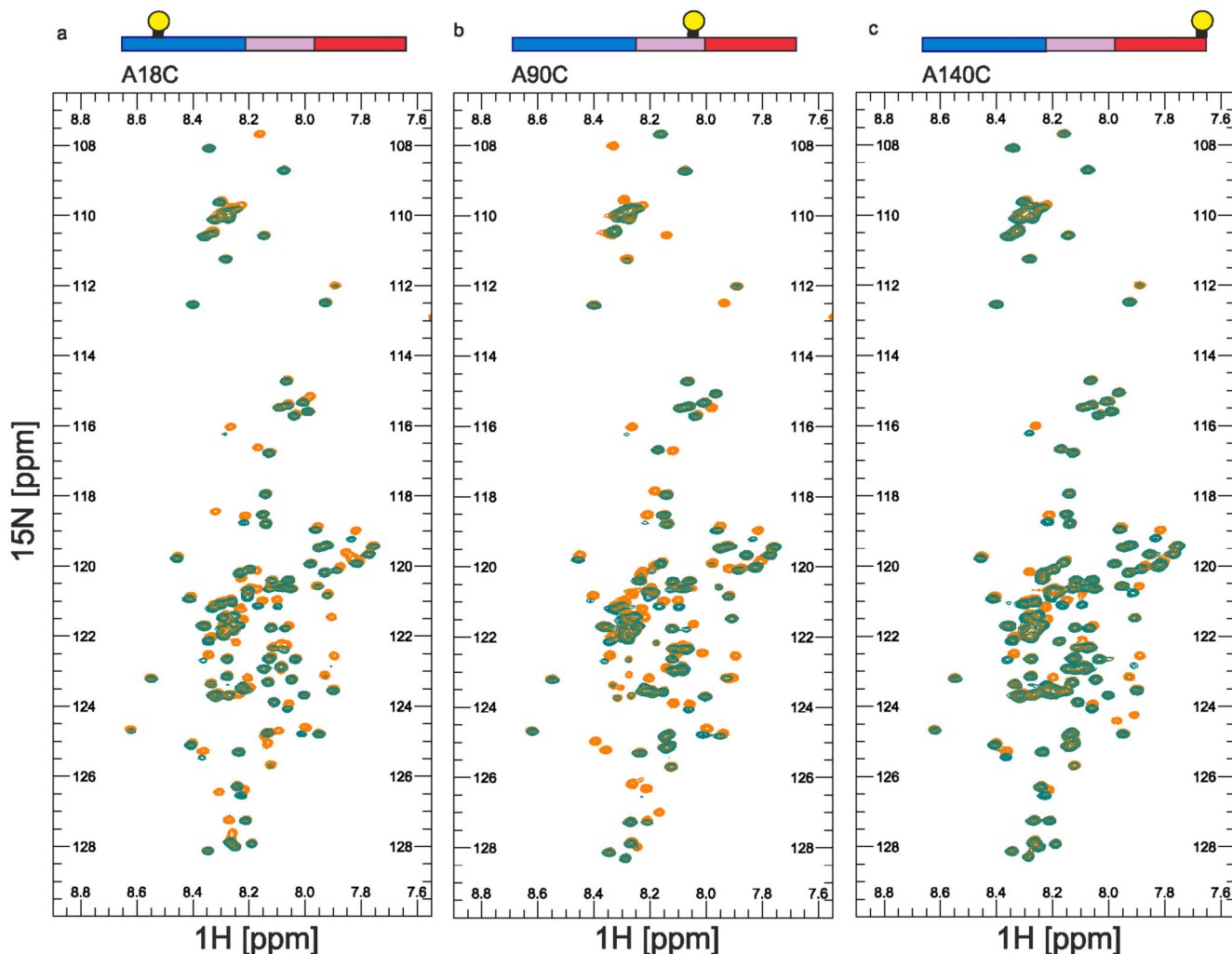


### Extended data Figure 3. Aggregation kinetics of C1 and P1P2-GS.

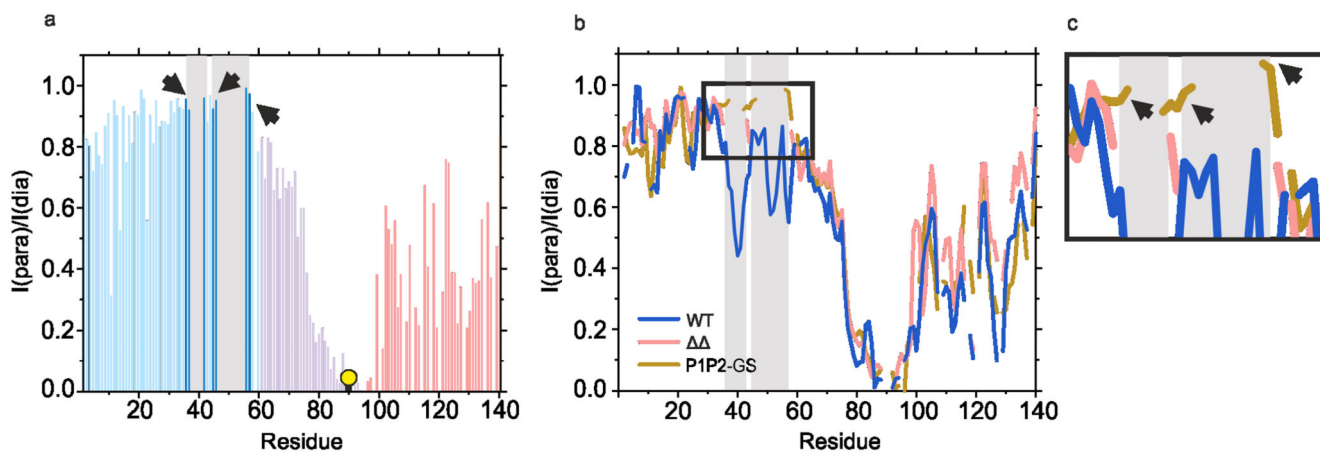
a) Schematic of WT, C1, and P1P2-GS  $\alpha$ Syn variants including the amino acid sequence of deleted C1 region and substituted P1/P2 region. ThT assays at pH 4.5 or pH 7.5 of b,c) WT  $\alpha$ Syn, d,e) C1 (14-20), or f,g) P1P2-GS (dark and light colours depict assays in high (200 mM added NaCl) or low (20 mM added NaCl) conditions, respectively (n = 3). h,i) Negative stain TEM images of representative samples at the endpoint (100 h) of the incubation of h) C1 or i) P1P2-GS, with colour coding consistent with c-f. Scale bars are



200 nm. The fibril yield under each condition, determined by SDS PAGE subsequent to centrifugation (see Methods) is shown in Supplementary Table S1.

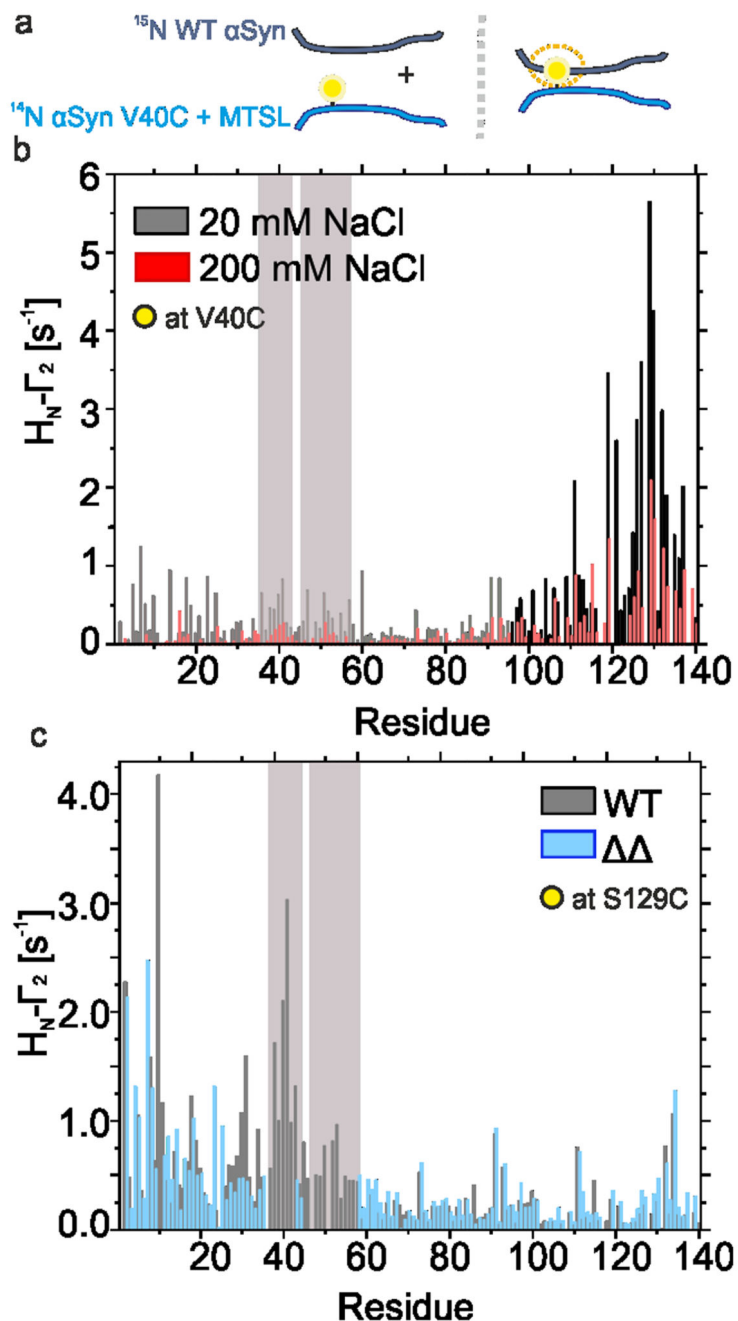


**Extended data Figure 4.  $^1\text{H}$ - $^{15}\text{N}$  HSQC NMR spectra showing intramolecular PRE NMR experiments on WT  $\alpha\text{Syn}$  in 20 mM sodium acetate buffer, 20 mM NaCl, pH 4.5, 15 °C.** Overlaid are paramagnetic (green) and diamagnetic (orange) spectra for WT  $\alpha\text{Syn}$  labelled at positions a) A18C, b) A90C or c) A140C. Schematics are shown above each spectrum with the N-terminal (blue), NAC (pink) and C-terminal (red) regions highlighted. The location of spin label is denoted by a yellow circle. Note that small chemical shift changes are observed upon reduction with ascorbic acid, which can be attributed to small changes in pH (see Methods). As a consequence 2 mM ascorbic acid was used throughout this study, resulting in incomplete reduction of the MTSL-labelled sample. This does not affect the pattern of PREs observed and results in an underestimate of the PRE effect (especially for residues in the NAC region as K80, G84, S87, I88, A89, K96, Q99).



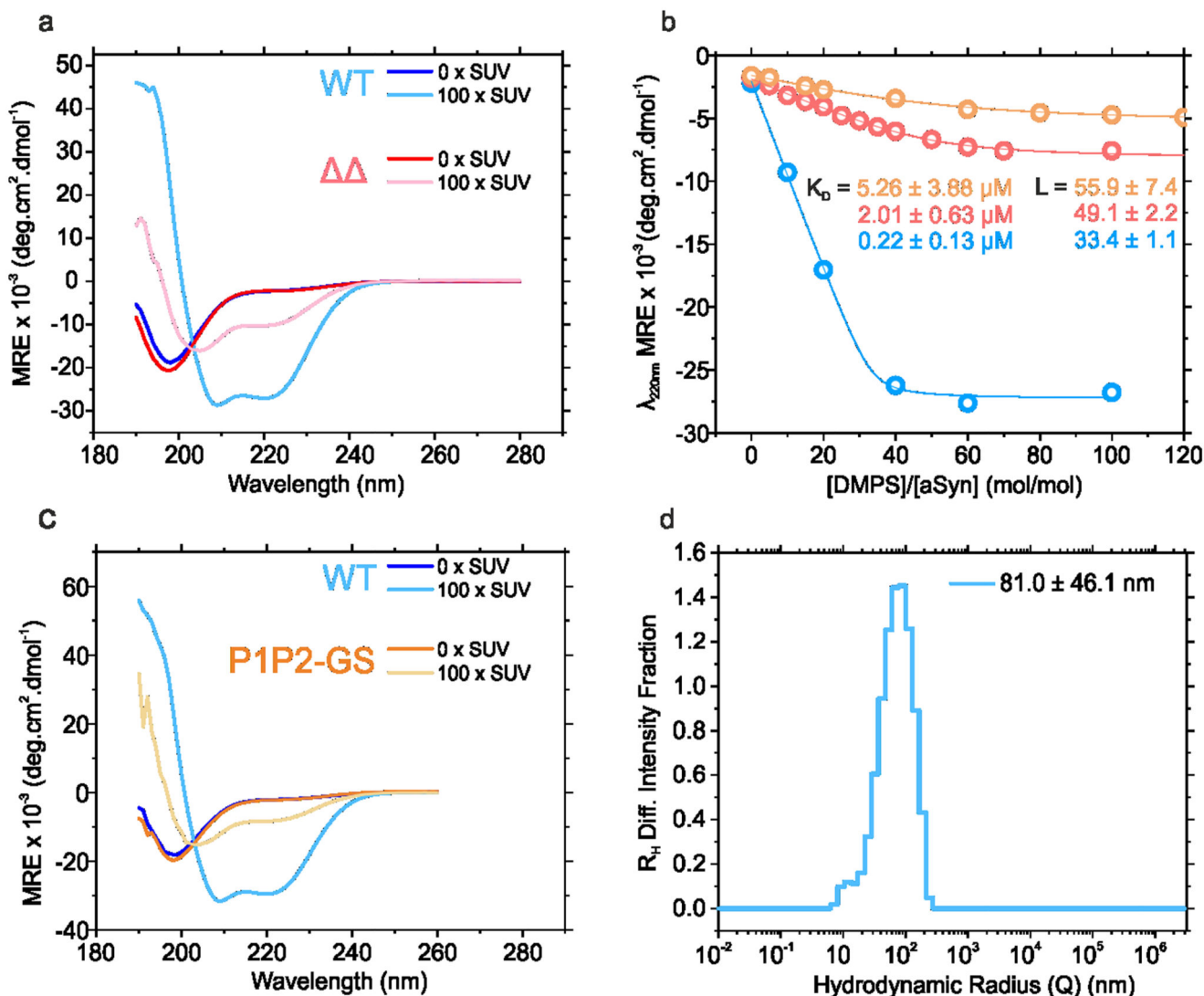
**Extended data Figure 5. Intramolecular PRE experiment for P1P2-GS  $\alpha$ Syn.**

a) Intramolecular PRE intensity ratios of amide protons (paramagnetic/diamagnetic) for P1P2-GS  $\alpha$ Syn with the MTSL spin label at A90C at low ionic strengths (20 mM NaCl), 15 °C, pH 4.5. Blue, pink and red bars show intensity ratios for residues in the N-terminal, NAC and C-terminal regions, respectively. Dark blue bars highlight residues in the P1/P2 regions that could be assigned and measured. The grey boxes mark the P1/P2 regions. Black arrows show only a small PRE effect is observed in the P1/P2 region for P1P2-GS. Due to the repeating Gly and Ser residues in the P1/P2 sequence not all residues could be assigned (Methods). b) Comparison of a rolling window (over 5 residues for easier comparison) of the PRE effects for WT (blue),  $\Delta\Delta$  (red) and P1P2-GS (orange)  $\alpha$ Syn. The black box is zoomed out in c) to highlight residues in the P1/P2-region. The data for WT and  $\Delta\Delta$  are shown in Figures 4d and 5d.



**Extended data Figure 6. The role of P1 and P2 in intermolecular interactions.**

a) Schematic of intermolecular PRE experiments.  $^{14}\text{N}$  and  $^{15}\text{N}$   $\alpha\text{Syn}$  are illustrated as cyan and dark blue chains, respectively. MTSL is shown as a yellow circle. b)  $H_{\text{N}}-\Gamma_2$  rates for WT  $\alpha\text{Syn}$  labelled with MTSL at position 40 (A40C) at pH 4.5 in low salt (20 mM added NaCl) (black) or high salt (200 mM added NaCl) (red) conditions, 15 °C. Bars depict residue specific  $H_{\text{N}}-\Gamma_2$  rates. c)  $H_{\text{N}}-\Gamma_2$  rates at pH 4.5 under low salt (20 mM added NaCl) for WT (black) or  $\Delta\Delta$  (blue)  $\alpha\text{Syn}$  labelled at position 129 (S129C). Bars depict residue-specific  $H_{\text{N}}-\Gamma_2$  rates.



Extended data Figure 7. CD binding assays of  $\alpha$ Syn WT,  $\Delta\Delta$  and P1P2-GS to DMPS LUVs.

a) Far-UV CD spectra of 25  $\mu$ M WT  $\alpha$ Syn (blue) or  $\Delta\Delta$  (red) incubated in the absence or presence of liposomes (100:1 (M/M) DMPS: $\alpha$ Syn). b) Change of CD signal of WT  $\alpha$ Syn (blue),  $\Delta\Delta$  (red) or P1P2-GS (orange) at 220 nm as a function of [DMPS]/[ $\alpha$ Syn] ratio. Data were fitted (solid lines) to a single-step binding model, yielding the affinity ( $K_D$ ) and stoichiometry value (L) (the number of DMPS molecules in the bilayer that are involved in binding to one molecule of  $\alpha$ Syn<sup>56</sup>). c) Far-UV CD spectra of 25  $\mu$ M WT  $\alpha$ Syn (blue) or P1P2-GS (orange) incubated in the absence or presence of 100-times molar excess of DMPS LUVs. d) Dynamic light scattering of DMPS liposomes showing they have a hydrodynamic radius ( $R_H$ ) of on 81 nm.

## Supplementary Material

Refer to Web version on PubMed Central for supplementary material.



## Acknowledgments

We thank members of our research groups for helpful discussions throughout this work. We also thank Theo Karamanos for helpful advice about NMR PRE data analysis, Ellen Nollen (University of Groningen) for the kind gift of the plasmid encoding YFP- $\alpha$ Syn, Leon Willis for help with SEC-MALS analysis, Bob Schiffrin for his help with the  $K_d$  fitting and the mass spectrometry facility for help with characterisation of all purified proteins. SER acknowledges funding from the European Research Council under the European Union's Seventh Framework Programme FP7.2007-2013/Grant agreement number 322408 and Wellcome Trust (204963). CPAD was supported by BBSRC (BB/K02101X/1) and by the ERC (322408), SCG by BBSRC (BB/M011151/1), RMM by Wellcome Trust (204963) and SMU by the Wellcome Trust (215062/Z/18/Z). PvOH is also funded N3CR grant (NC/P001203/1). We thank the Wellcome Trust (094232) and University of Leeds for the purchase of the Chiroscan CD spectrometer, the electron microscopes and NMR instrumentation.

## References

- Iwai A, Masliah E, Yoshimoto M, Ge NF, Flanagan L, et al. The precursor protein of non-a-beta component of Alzheimers-disease amyloid is a presynaptic protein of the central-nervous-system. *Neuron*. 1995; 14:467–475. [PubMed: 7857654]
- Dettmer U, Selkoe D, Bartels T. New insights into cellular alpha-synuclein homeostasis in health and disease. *Curr Opin Neurobiol*. 2016; 36:15–22. [PubMed: 26282834]
- Iadanza MG, Jackson MP, Hewitt EW, Ranson NA, Radford SE. A new era for understanding amyloid structures and disease. *Nat Rev Mol Cell Biol*. 2018
- Tysnes O-B, Storstein A. Epidemiology of Parkinson's disease. *J Neural Transm*. 2017; 124:901–905. [PubMed: 28150045]
- Weinreb PH, Zhen W, Poon AW, Conway KA, Lansbury PT. NACP, a protein implicated in Alzheimer's disease and learning, is natively unfolded. *Biochemistry*. 1996; 35:13709–13715. [PubMed: 8901511]
- Theillet F-X, Binolfi A, Bekei B, Martorana A, Rose HM, et al. Structural disorder of monomeric  $\alpha$ -synuclein persists in mammalian cells. *Nature*. 2016; 530:45. [PubMed: 26808899]
- Fusco G, Chen SW, Williamson PTF, Cascella R, Perni M, et al. Structural basis of membrane disruption and cellular toxicity by  $\alpha$ -synuclein oligomers. *Science*. 2017; 358:1440–1443. [PubMed: 29242346]
- Chen SW, Drakulic S, Deas E, Ouberai M, Aprile FA, et al. Structural characterization of toxic oligomers that are kinetically trapped during alpha-synuclein fibril formation. *Proc Natl Acad Sci U S A*. 2015; 112:E1994–2003. [PubMed: 25855634]
- Peelaerts W, Bousset L, Van der Perren A, Moskalyuk A, Pulizzi R, et al. Alpha-synuclein strains cause distinct synucleinopathies after local and systemic administration. *Nature*. 2015; 522:340–+. [PubMed: 26061766]
- Bartels T, Ahlstrom LS, Leftin A, Kamp F, Haass C, et al. The N-terminus of the intrinsically disordered protein  $\alpha$ -synuclein triggers membrane binding and helix folding. *Biophys J*. 2010; 99:2116–2124. [PubMed: 20923645]
- Salveson PJ, Spencer RK, Nowick JS. X-ray crystallographic structure of oligomers formed by a toxic  $\beta$ -hairpin derived from  $\alpha$ -synuclein: Trimers and higher-order oligomers. *J Am Chem Soc*. 2016; 138:4458–4467. [PubMed: 26926877]
- Giasson BI, Murray IV, Trojanowski JQ, Lee VM. A hydrophobic stretch of 12 amino acid residues in the middle of alpha-synuclein is essential for filament assembly. *J Biol Chem*. 2001; 276:2380–6. [PubMed: 11060312]
- Li B, Ge P, Murray KA, Sheth P, Zhang M, et al. Cryo-em of full-length  $\alpha$ -synuclein reveals fibril polymorphs with a common structural kernel. *Nat Commun*. 2018; 9:3609. [PubMed: 30190461]
- Guerrero-Ferreira R, Taylor NMI, Mona D, Ringler P, Lauer ME, et al. Cryo-EM structure of alpha-synuclein fibrils. *Elife*. 2018; 7
- Tuttle MD, Comellas G, Nieuwkoop AJ, Covell DJ, Berthold DA, et al. Solid-state NMR structure of a pathogenic fibril of full-length human alpha-synuclein. *Nat Struct Mol Biol*. 2016; 23:409–15. [PubMed: 27018801]

16. Allison JR, Varnai P, Dobson CM, Vendruscolo M. Determination of the free energy landscape of alpha-synuclein using spin label nuclear magnetic resonance measurements. *J Am Chem Soc.* 2009; 131:18314–18326. [PubMed: 20028147]
17. Bertoncini CW, Jung YS, Fernandez CO, Hoyer W, Griesinger C, et al. Release of long-range tertiary interactions potentiates aggregation of natively unstructured alpha-synuclein. *Proc Natl Acad Sci U S A.* 2005; 102:1430–1435. [PubMed: 15671169]
18. Rao JN, Jao CC, Hegde BG, Langen R, Ulmer TS. A combinatorial nmr and EPR approach for evaluating the structural ensemble of partially folded proteins. *J Am Chem Soc.* 2010; 132:8657–8668. [PubMed: 20524659]
19. Phillips AS, Gomes AF, Kalapothakis JM, Gillam JE, Gasparavicius J, et al. Conformational dynamics of  $\alpha$ -synuclein: Insights from mass spectrometry. *Analyst.* 2015; 140:3070–3081. [PubMed: 25756329]
20. Uversky VN, Li J, Fink AL. Evidence for a partially folded intermediate in alpha-synuclein fibril formation. *J Biol Chem.* 2001; 276:10737–10744. [PubMed: 11152691]
21. Wu KP, Weinstock DS, Narayanan C, Levy RM, Baum J. Structural reorganization of alpha-synuclein at low pH observed by NMR and REMD simulations. *J Mol Biol.* 2009; 391:784–796. [PubMed: 19576220]
22. Hoyer W, Cherny D, Subramaniam V, Jovin TM. Impact of the acidic C-terminal region comprising amino acids 109–140 on  $\alpha$ -synuclein aggregation in vitro. *Biochemistry.* 2004; 43:16233–16242. [PubMed: 15610017]
23. Stephens AD, Zacharopoulou M, Kaminski Schierle GS. The cellular environment affects monomeric  $\alpha$ -synuclein structure. *Trends Biochem Sci.* 2018
24. Das M, Mei X, Jayaraman S, Atkinson D, Gursky O. Amyloidogenic mutations in human apolipoprotein A-I are not necessarily destabilizing—a common mechanism of apolipoprotein A-I misfolding in familial amyloidosis and atherosclerosis. *The FEBS journal.* 2014; 281:2525–2542. [PubMed: 24702826]
25. Hoop CL, Lin H-K, Kar K, Hou Z, Poirier MA, et al. Polyglutamine amyloid core boundaries and flanking domain dynamics in huntingtin fragment fibrils determined by solid-state nuclear magnetic resonance. *Biochemistry.* 2014; 53:6653–6666. [PubMed: 25280367]
26. Bugg CW, Isas JM, Fischer T, Patterson PH, Langen R. Structural features and domain organization of huntingtin fibrils. *J Biol Chem.* 2012; 287:31739–31746. [PubMed: 22801429]
27. Colvin MT, Silvers R, Ni QZ, Can TV, Sergeyev I, et al. Atomic resolution structure of monomeric A $\beta$ 42 amyloid fibrils. *J Am Chem Soc.* 2016; 138:9663–9674. [PubMed: 27355699]
28. Lucato CM, Lupton CJ, Halls ML, Ellisdon AM. Amyloidogenicity at a distance: How distal protein regions modulate aggregation in disease. *J Mol Biol.* 2017; 429:1289–1304. [PubMed: 28342736]
29. Crowther RA, Jakes R, Spillantini MG, Goedert M. Synthetic filaments assembled from C-terminally truncated  $\alpha$ -synuclein. *FEBS Lett.* 1998; 436:309–312. [PubMed: 9801138]
30. Kessler JC, Rochet J-C, Lansbury PT. The N-terminal repeat domain of  $\alpha$ -synuclein inhibits  $\beta$ -sheet and amyloid fibril formation. *Biochemistry.* 2003; 42:672–678. [PubMed: 12534279]
31. Izawa Y, Tateno H, Kameda H, Hirakawa K, Hato K, et al. Role of C-terminal negative charges and tyrosine residues in fibril formation of alpha-synuclein. *Brain and Behavior.* 2012; 2:595–605. [PubMed: 23139905]
32. Rodriguez JA, Ivanova MI, Sawaya MR, Cascio D, Reyes FE, et al. Structure of the toxic core of alpha-synuclein from invisible crystals. *Nature.* 2015; 525:486–90. [PubMed: 26352473]
33. Li Y, Zhao C, Luo F, Liu Z, Gui X, et al. Amyloid fibril structure of  $\alpha$ -synuclein determined by cryo-electron microscopy. *Cell Res.* 2018; 28:897. [PubMed: 30065316]
34. Van Ham TJ, Thijssen KL, Breitling R, Hofstra RM, Plasterk RH, et al. C. Elegans model identifies genetic modifiers of  $\alpha$ -synuclein inclusion formation during aging. *PLoS genetics.* 2008; 4:e1000027. [PubMed: 18369446]
35. Fusco G, Pape T, Stephens AD, Mahou P, Costa AR, et al. Structural basis of synaptic vesicle assembly promoted by alpha-synuclein. *Nat Commun.* 2016; 7

36. Lautenschläger J, Stephens AD, Fusco G, Ströhl F, Curry N, et al. C-terminal calcium binding of  $\alpha$ -synuclein modulates synaptic vesicle interaction. *Nat Commun.* 2018; 9:712. [PubMed: 29459792]
37. Tartaglia GG, Vendruscolo M. The Zygggregator method for predicting protein aggregation propensities. *Chem Soc Rev.* 2008; 37:1395–1401. [PubMed: 18568165]
38. Sormanni P, Aprile FA, Vendruscolo M. The camsol method of rational design of protein mutants with enhanced solubility. *J Mol Biol.* 2015; 427:478–490. [PubMed: 25451785]
39. Thompson MJ, Sievers SA, Karanicolas J, Ivanova MI, Baker D, et al. The 3D profile method for identifying fibril-forming segments of proteins. *Proc Natl Acad Sci U S A.* 2006; 103:4074–4078. [PubMed: 16537487]
40. Terada M, Suzuki G, Nonaka T, Kametani F, Tamaoka A, et al. The effect of truncation on prion-like properties of  $\alpha$ -synuclein. *J Biol Chem.* 2018; 293:13910–13920. [PubMed: 30030380]
41. Mirecka EA, Shaykhalishahi H, Gauhar A, Akgul S, Lecher J, et al. Sequestration of a beta-hairpin for control of alpha-synuclein aggregation. *Angew Chem Int Ed Engl.* 2014; 53:4227–30. [PubMed: 24623599]
42. Shaykhalishahi H, Gauhar A, Wordehoff MM, Gruning CS, Klein AN, et al. Contact between the beta1 and beta2 segments of alpha-synuclein that inhibits amyloid formation. *Angew Chem Int Ed Engl.* 2015; 54:8837–40. [PubMed: 26119103]
43. Agerschou ED, Saridaki T, Flagmeier P, Galvagnion C, Komnig D, et al. An engineered monomer binding-protein for  $\alpha$ -synuclein efficiently inhibits the proliferation of amyloid fibrils. *Elife.* 2019; 8:e46112. [PubMed: 31389332]
44. Cho MK, Nodet G, Kim HY, Jensen MR, Bernado P, et al. Structural characterization of  $\alpha$ -synuclein in an aggregation prone state. *Protein Sci.* 2009; 18:1840–1846. [PubMed: 19554627]
45. Buell AK, Galvagnion C, Gaspar R, Sparr E, Vendruscolo M, et al. Solution conditions determine the relative importance of nucleation and growth processes in  $\alpha$ -synuclein aggregation. *Proc Natl Acad Sci.* 2014; 111:7671–7676. [PubMed: 24817693]
46. Hoyer W, Antony T, Cherny D, Heim G, Jovin TM, et al. Dependence of  $\alpha$ -synuclein aggregate morphology on solution conditions. *J Mol Biol.* 2002; 322:383–393. [PubMed: 12217698]
47. Wördehoff MM, Shaykhalishahi H, Groß L, Gremer L, Stoldt M, et al. Opposed effects of dityrosine formation in soluble and aggregated  $\alpha$ -synuclein on fibril growth. *J Mol Biol.* 2017; 429:3018–3030. [PubMed: 28918091]
48. Wu K-P, Baum J. Detection of transient interchain interactions in the intrinsically disordered protein  $\alpha$ -synuclein by nmr paramagnetic relaxation enhancement. *J Am Chem Soc.* 2010; 132:5546–5547. [PubMed: 20359221]
49. Dedmon MM, Lindorff-Larsen K, Christodoulou J, Vendruscolo M, Dobson CM. Mapping long-range interactions in  $\alpha$ -synuclein using spin-label NMR and ensemble molecular dynamics simulations. *J Am Chem Soc.* 2005; 127:476–477. [PubMed: 15643843]
50. Wu K-P, Kim S, Fela DA, Baum J. Characterization of conformational and dynamic properties of natively unfolded human and mouse  $\alpha$ -synuclein ensembles by NMR: Implication for aggregation. *J Mol Biol.* 2008; 378:1104–1115. [PubMed: 18423664]
51. Bertoncini CW, Fernandez CO, Griesinger C, Jovin TM, Zweckstetter M. Familial mutants of  $\alpha$ -synuclein with increased neurotoxicity have a destabilized conformation. *J Biol Chem.* 2005; 280:30649–30652. [PubMed: 16020550]
52. Sung, Y-h; Eliezer, D. Residual structure, backbone dynamics, and interactions within the synuclein family. *J Mol Biol.* 2007; 372:689. [PubMed: 17681534]
53. Esteban-Martín S, Silvestre-Ryan J, Bertoncini CW, Salvatella X. Identification of fibril-like tertiary contacts in soluble monomeric  $\alpha$ -synuclein. *Biophys J.* 2013; 105:1192–1198. [PubMed: 24010662]
54. Janowska MK, Wu K-P, Baum J. Unveiling transient protein-protein interactions that modulate inhibition of alpha-synuclein aggregation by beta-synuclein, a pre-synaptic protein that co-localizes with alpha-synuclein. *Scientific reports.* 2015; 5:15164–15164. [PubMed: 26477939]
55. Ben-Zvi A, Miller EA, Morimoto RI. Collapse of proteostasis represents an early molecular event in *Caenorhabditis elegans* aging. *Proc Natl Acad Sci.* 2009; 106:14914–14919. [PubMed: 19706382]

56. Labbadia J, Morimoto RI. Repression of the heat shock response is a programmed event at the onset of reproduction. *Mol Cell*. 2015; 59:639–650. [PubMed: 26212459]
57. Diao J, Burré J, Vivona S, Cipriano DJ, Sharma M, et al. Native  $\alpha$ -synuclein induces clustering of synaptic-vesicle mimics via binding to phospholipids and synaptobrevin-2/VAMP2. *Elife*. 2013; 2:e00592. [PubMed: 23638301]
58. Bodner CR, Dobson CM, Bax A. Multiple tight phospholipid-binding modes of  $\alpha$ -synuclein revealed by solution NMR spectroscopy. *J Mol Biol*. 2009; 390:775–790. [PubMed: 19481095]
59. Fusco G, De Simone A, Gopinath T, Vostrikov V, Vendruscolo M, et al. Direct observation of the three regions in  $\alpha$ -synuclein that determine its membrane-bound behaviour. *Nat Commun*. 2014; 5:3827. [PubMed: 24871041]
60. Jao CC, Hegde BG, Chen J, Haworth IS, Langen R. Structure of membrane-bound  $\alpha$ -synuclein from site-directed spin labeling and computational refinement. *Proc Natl Acad Sci*. 2008; 105:19666–19671. [PubMed: 19066219]
61. Galvagnion C, Buell AK, Meisl G, Michaels TC, Vendruscolo M, et al. Lipid vesicles trigger alpha-synuclein aggregation by stimulating primary nucleation. *Nat Chem Biol*. 2015; 11:229–34. [PubMed: 25643172]
62. Fonseca-Ornelas L, Eisbach SE, Paulat M, Giller K, Fernández CO, et al. Small molecule-mediated stabilization of vesicle-associated helical  $\alpha$ -synuclein inhibits pathogenic misfolding and aggregation. *Nat Commun*. 2014; 5:5857. [PubMed: 25524885]
63. Jackson MP, Hewitt EW. Cellular proteostasis: Degradation of misfolded proteins by lysosomes. *Essays Biochem*. 2016; 60:173–180. [PubMed: 27744333]
64. Brännström K, Öhman A, Nilsson L, Pihl M, Sandblad L, et al. The N-terminal region of amyloid  $\beta$  controls the aggregation rate and fibril stability at low pH through a gain of function mechanism. *J Am Chem Soc*. 2014; 136:10956–10964. [PubMed: 25014209]
65. Chen D, Drombosky KW, Hou Z, Sari L, Kashmer OM, et al. Tau local structure shields an amyloid-forming motif and controls aggregation propensity. *Nat Commun*. 2019; 10:2493. [PubMed: 31175300]
66. Esposito G, Michelutti R, Verdone G, Viglino P, Hernandez H, et al. Removal of the N-terminal hexapeptide from human  $\beta$ 2-microglobulin facilitates protein aggregation and fibril formation. *Protein Sci*. 2000; 9:831–845. [PubMed: 10850793]
67. Goedert M. Alpha-synuclein and neurodegenerative diseases. *Nat Rev Neurosci*. 2001; 2:492. [PubMed: 11433374]
68. Mehra S, Sahay S, Maji SK.  $\alpha$ -synuclein misfolding and aggregation: Implications in Parkinson's disease pathogenesis. *Biochimica et Biophysica Acta (BBA)-Proteins and Proteomics*. 2019
69. Cabin DE, Shimazu K, Murphy D, Cole NB, Gottschalk W, et al. Synaptic vesicle depletion correlates with attenuated synaptic responses to prolonged repetitive stimulation in mice lacking  $\alpha$ -synuclein. *J Neurosci*. 2002; 22:8797–8807. [PubMed: 12388586]
70. Martin EM, Jackson MP, Gamerding M, Gense K, Karamonos TK, et al. Conformational flexibility within the nascent polypeptide-associated complex enables its interactions with structurally diverse client proteins. *The Journal of biological chemistry*. 2018; 293:8554–8568. [PubMed: 29650757]
71. Masuda M, Dohmae N, Nonaka T, Oikawa T, Hisanaga S-i, et al. Cysteine misincorporation in bacterially expressed human  $\alpha$ -synuclein. *FEBS Lett*. 2006; 580:1775–1779. [PubMed: 16513114]
72. Delaglio F, Grzesiek S, Vuister GW, Zhu G, Pfeifer J, et al. NMRPipe: A multidimensional spectral processing system based on UNIX pipes. *J BioMol NMR*. 1995; 6:277–293. [PubMed: 8520220]
73. Skinner SP, Fogh RH, Boucher W, Ragan TJ, Mureddu LG, et al. CcpNmr analysisassign: A flexible platform for integrated NMR analysis. *J BioMol NMR*. 2016; 66:111–124. [PubMed: 27663422]
74. Fogh R, Ionides J, Ulrich E, Boucher W, Vranken W, et al. The ccpn project: An interim report on a data model for the NMR community. *Nat Struct Mol Biol*. 2002; 9:416.
75. Tang C, Schwieters CD, Clore GM. Open-to-closed transition in apo maltose-binding protein observed by paramagnetic NMR. *Nature*. 2007; 449:1078. [PubMed: 17960247]
76. Brenner S. The genetics of *Caenorhabditis elegans*. *Genetics*. 1974; 77:71–94. [PubMed: 4366476]

77. Nussbaum-Krammer CI, Neto MF, Brielmann RM, Pedersen JS, Morimoto RI. Investigating the spreading and toxicity of prion-like proteins using the metazoan model organism *C. elegans*. *JoVE (Journal of Visualized Experiments)*. 2015:e52321.
78. Whitmore L, Wallace B. Dichroweb, an online server for protein secondary structure analyses from circular dichroism spectroscopic data. *Nucleic Acids Res.* 2004; 32:W668–W673. [PubMed: 15215473]

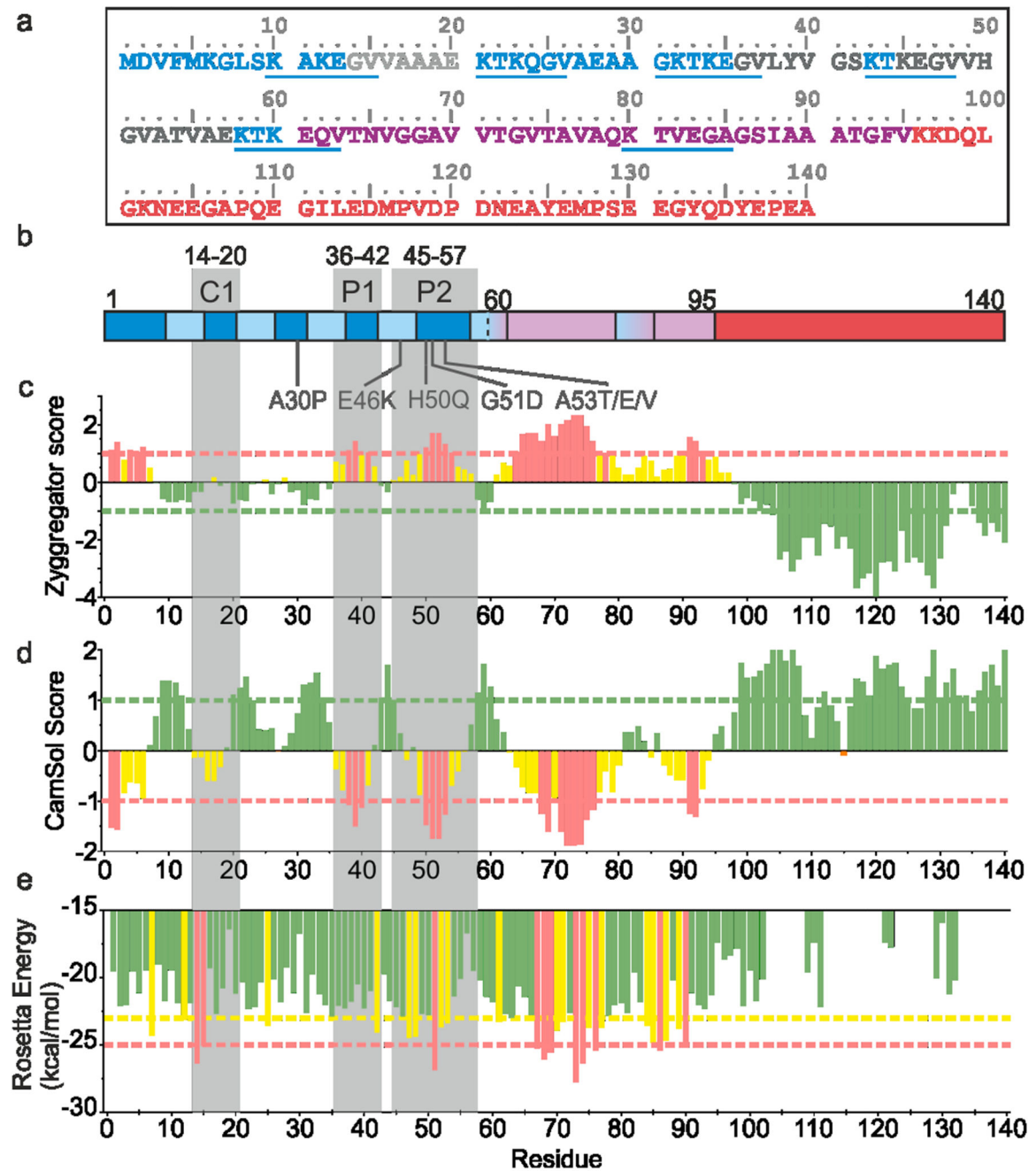


**Figure 1. Aggregation and solubility profiles of  $\alpha$ Syn.**

a) The sequence of human  $\alpha$ Syn. The N-terminal region (1-60), NAC region (61-95) and C-terminal region (96-140) are coloured in blue, pink, and red, respectively. The C1 and P1/P2 regions shown in (b) are coloured pale grey and dark grey respectively. The imperfect KTKEGV repeats are underlined in blue. b) Regions of  $\alpha$ Syn highlighting the imperfect KTKEGV repeats in the N-terminal region (light blue), the positions of the seven familial PD mutants, and the P1, P2 and C1 control sequence highlighted as in (a). c), d) and e) Zyggregator<sup>37</sup>, CamSol<sup>38</sup> and ZipperDB<sup>39</sup> profiles for the  $\alpha$ Syn sequence, respectively. Red



bars indicate aggregation-prone/low solubility regions. Yellow bars indicate residues with a higher than average aggregation propensity/low solubility, but which do not meet the threshold. Red dashed lines indicate the low solubility/high aggregation propensity threshold, while green dashed lines show threshold values for high solubility/low aggregation propensity. For Zipper DB, the yellow dashed line shows the threshold value of residues with a high probability of  $\beta$ -zipper formation<sup>39</sup>. Data for graphs in c-e are available as Source Data.

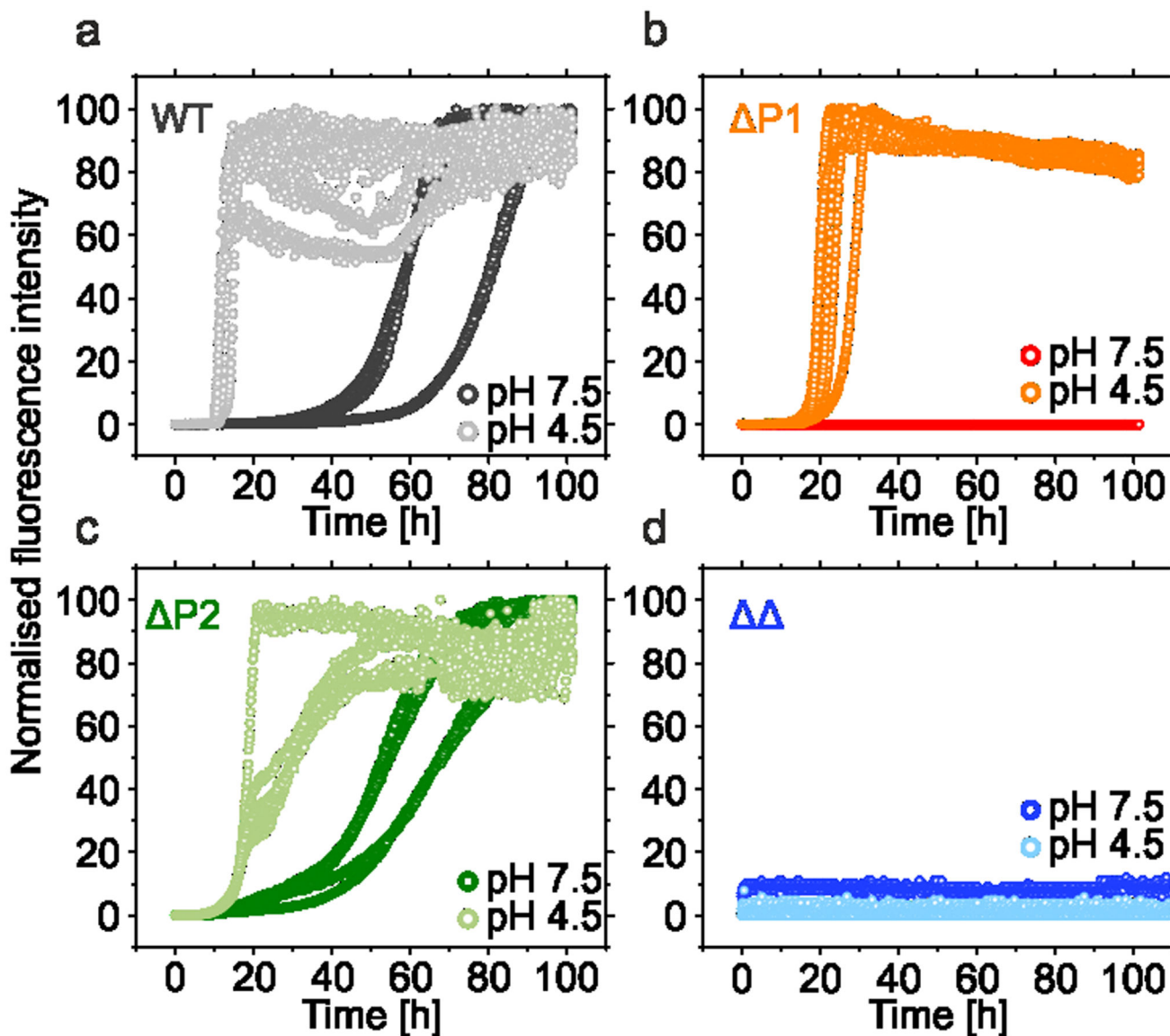
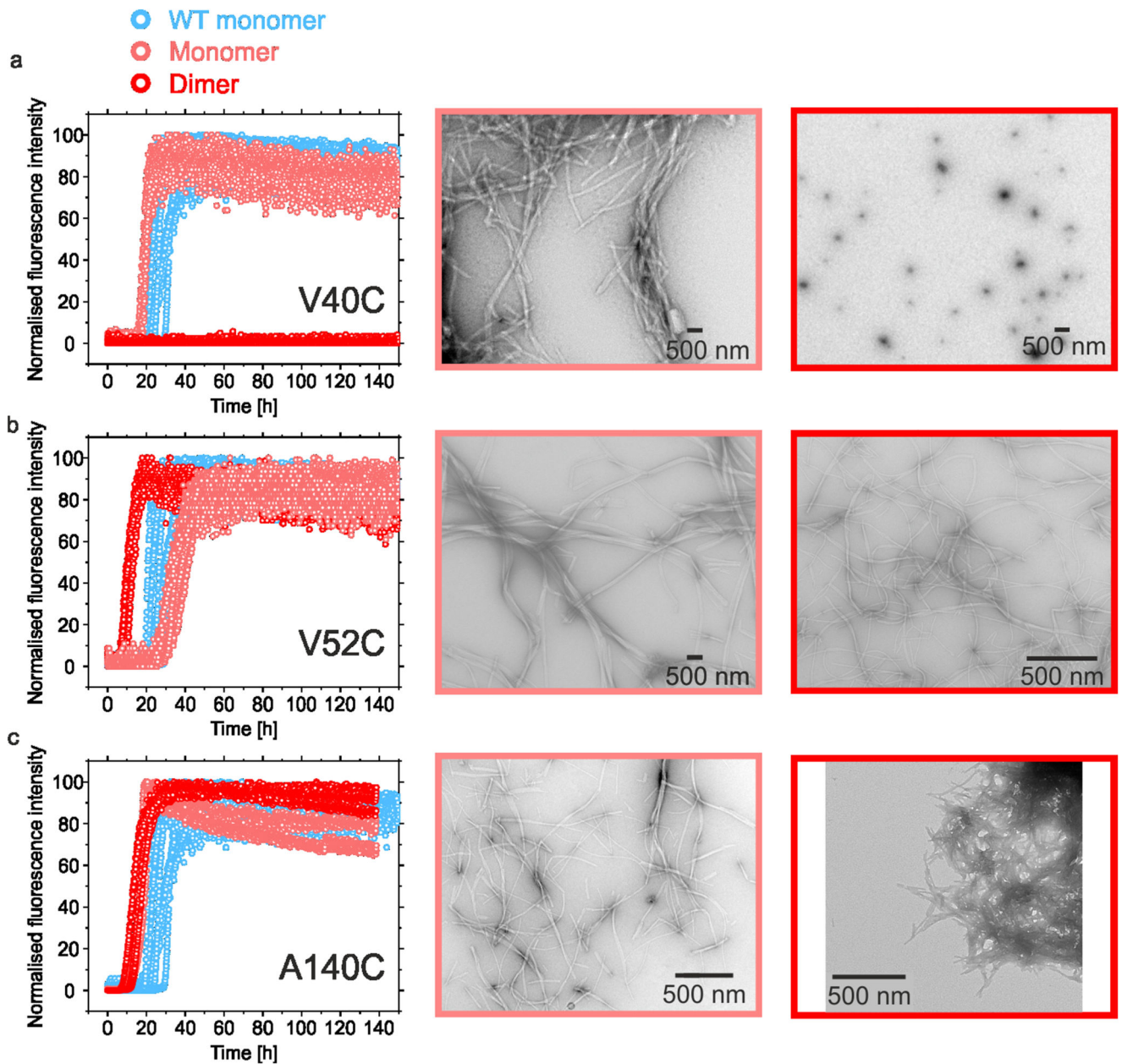


**Figure 2. The kinetics of aggregation of WT  $\alpha$ Syn and P1/P2 deletion variants.**

a-d The aggregation kinetics of 100  $\mu$ M WT  $\alpha$ Syn (a); P1 (b); P2 (c) or  $\Delta\Delta$  variants (d). Dark and light colours denote incubations carried out at pH 7.5 (20 mM Tris HCl, 200 mM NaCl, pH 7.5) or pH 4.5 (20 mM sodium acetate, 200 mM NaCl, pH 4.5), respectively. All experiments were carried out at 37 °C with agitation at 600 rpm and measured in at least triplicate. Lag times and elongation rates were determined for every single curve using OriginPro (see Methods), means and s.d. are listed in Supplementary Table 1. The fibril yield under each condition, determined by SDS PAGE subsequent to centrifugation (see Methods), is shown in Supplementary Table 1. Data for all graphs are available as Source Data.



samples), 37 °C with agitation at 600 rpm. Data for all ThT graphs are available as Source Data.

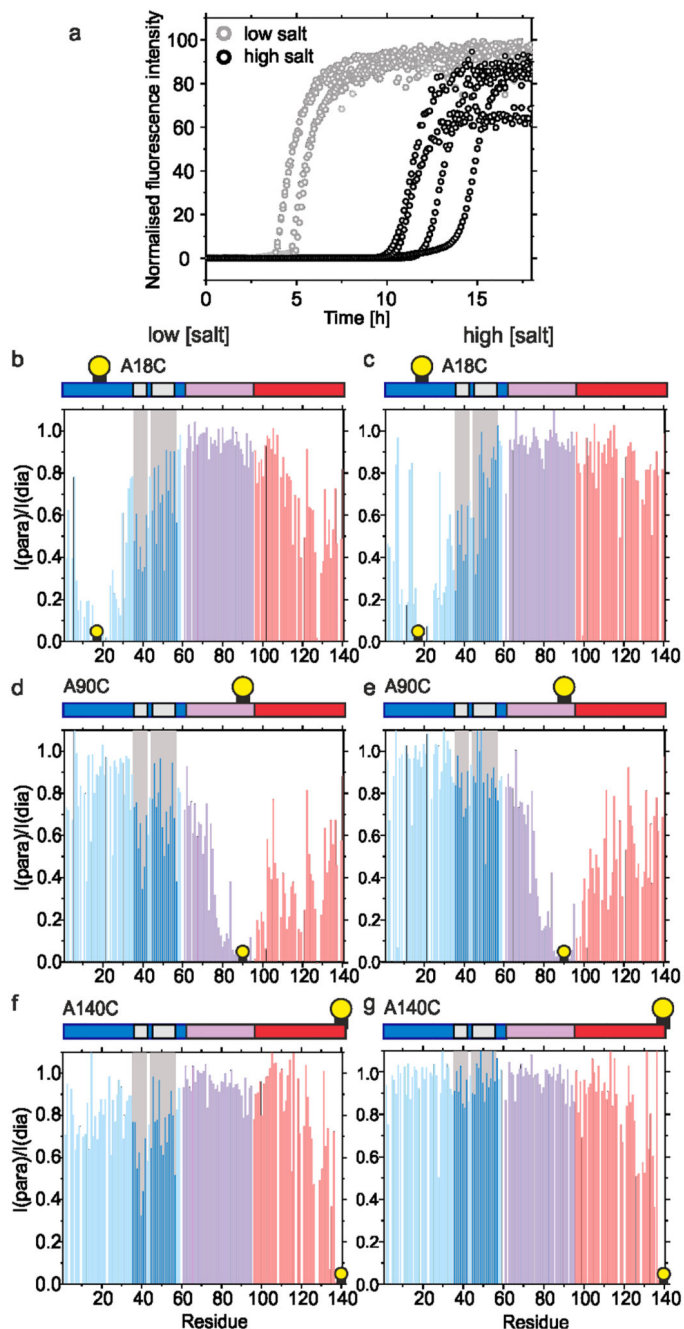


**Figure 4. Intramolecular PRE experiments for WT  $\alpha$ Syn.**

a) Aggregation kinetics (note the short timescale depicted) of WT  $\alpha$ Syn (100  $\mu$ M in 20 mM sodium acetate, pH 4.5, at low (20 mM added NaCl) or high (200 mM added NaCl) ionic strength at 37 °C). b-g Intramolecular PRE intensity ratios of amide protons (paramagnetic/diamagnetic) for WT  $\alpha$ Syn variants with MTSL spin labels at A18C (b,c), A90C (d,e) or A140C (f,g) at low (b,d,f) or high (c,e,g) ionic strengths, 15 °C, as indicated. Blue, pink and red bars show intensity ratios for the N-terminal, NAC and C-terminal regions, respectively. Dark blue bars highlighted in grey point out the position of the P1/P2 region. Schematics are

shown above each plot with a consistent colour scheme. The location of spin labels are denoted by a yellow circle. Grey panels highlight the location of the P1/P2 regions. Data for all graphs are available as Source Data.



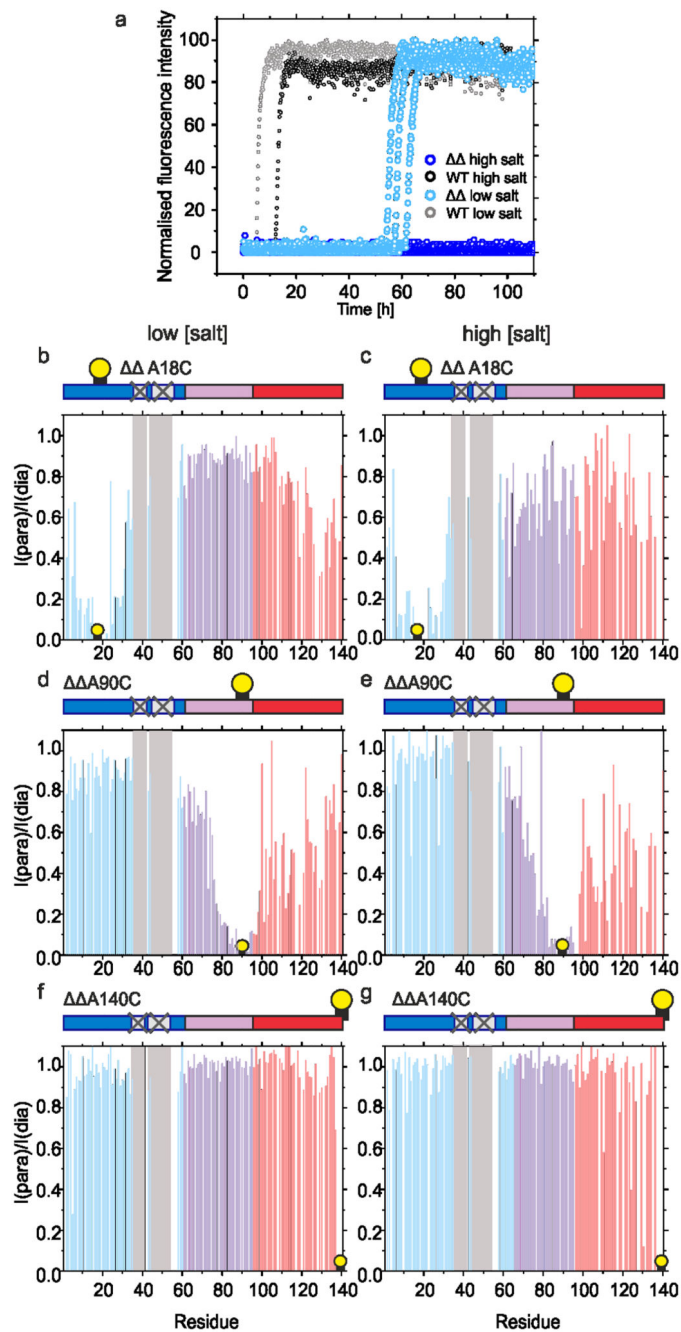


**Figure 5. Intramolecular PRE experiments for  $\alpha$ Syn.**

a) Aggregation kinetics (note different timescale compared with Extended Data Figure 1) of  $\Delta\Delta$  and WT  $\alpha$ Syn (100  $\mu$ M in 20 mM sodium acetate, pH 4.5, 37  $^{\circ}$ C at low (20 mM added NaCl) or high (200 mM added NaCl) ionic strength). b-g) Intramolecular PRE intensity ratios of amide protons (paramagnetic/diamagnetic) for variants with MTSL spin labels at A18C (b,c), A90C (d,e) or A140C (f,g) at low (b,d,f) or high (c,e,g) ionic strengths, at 15  $^{\circ}$ C, as indicated. Data for all graphs are available as Source Data.

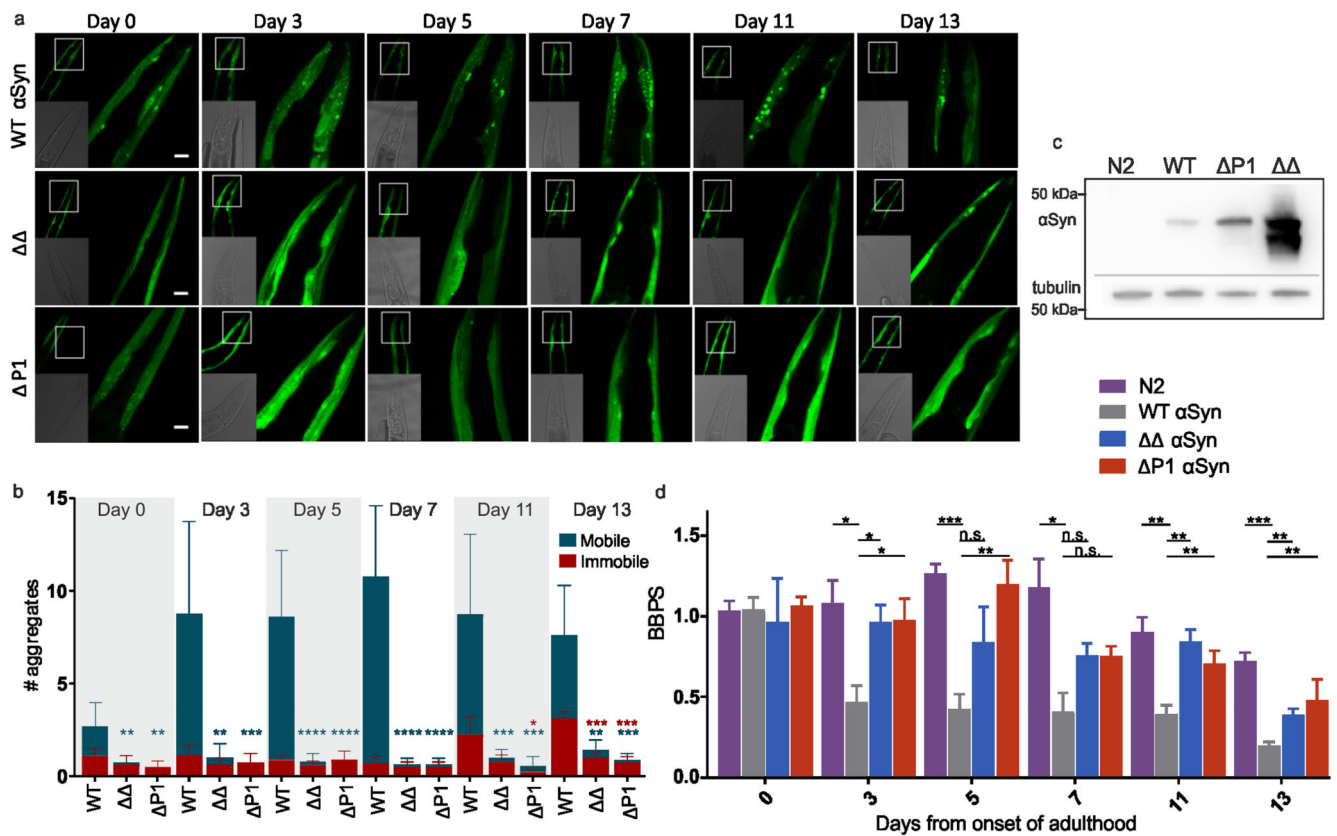


**Figure 6. Deletion of P1 or P1/P2 in *C. elegans* expressing  $\alpha$ Syn::YFP suppresses aggregation and proteotoxicity.**

a) Confocal microscopy images showing the head region of transgenic *C. elegans* expressing WT  $\alpha$ Syn,  $\Delta\Delta$ , or  $\Delta P1$  tagged C-terminally to YFP in the bodywall muscle during ageing (Day 0 to Day 13 of adulthood). Scale bar, 10  $\mu$ m. b) Number of mobile and immobile inclusions larger than  $\sim 2 \mu\text{m}^2$  per animal between the tip of the nose and pharyngeal bulb during ageing determined using FRAP. Data shown are the mean and s.e.m. for three independent experiments (biological replicates); in each experiment, 10 worms ( $n = 10$ ) were assessed for each time point. (n=10 worms). Blue stars indicate significance between the number of mobile aggregates of animals expressing WT  $\alpha$ Syn or the variants  $\Delta P1$  or  $\Delta\Delta$ . Red stars indicate significance between the number of immobile aggregates exhibited in animals expressing WT  $\alpha$ Syn compared with mutant animals. \* $P < 0.05$ ; \*\* $P < 0.01$ ; \*\*\* $P < 0.001$ ; \*\*\*\* $P < 0.0001$ . A one-sided Student's t test was used in all cases. c) Western blot analysis of protein extracts isolated from N2, WT  $\alpha$ Syn::YFP,  $\Delta P1$ ::YFP and  $\Delta\Delta$ ::YFP animals using an anti- $\alpha$ Syn antibody (Methods). Tubulin was used as a loading control. The loading control (anti-tubulin) was run on a different gel/membranes loaded with the same protein sample and treated and analysed in the same manner. The images were cropped showing all relevant bands. d) Number of body bends per second (BBPS) of N2, WT  $\alpha$ Syn::YFP,  $\Delta P1$ ::YFP and  $\Delta\Delta$ ::YFP animals from Day 0 (L4 stage) through to Day 13 of adulthood. Data shown are mean and s.e.m. for three independent experiment; in each experiment, 10 worms were assessed for each time point. n=10 for each experiment and

error bars represent SEM of three biological replicates. n.s. = not significant; \*\* $P < 0.01$ ; \* $P < 0.05$ , a one-sided test was used. Data for graphs in b-d are available as Source Data.

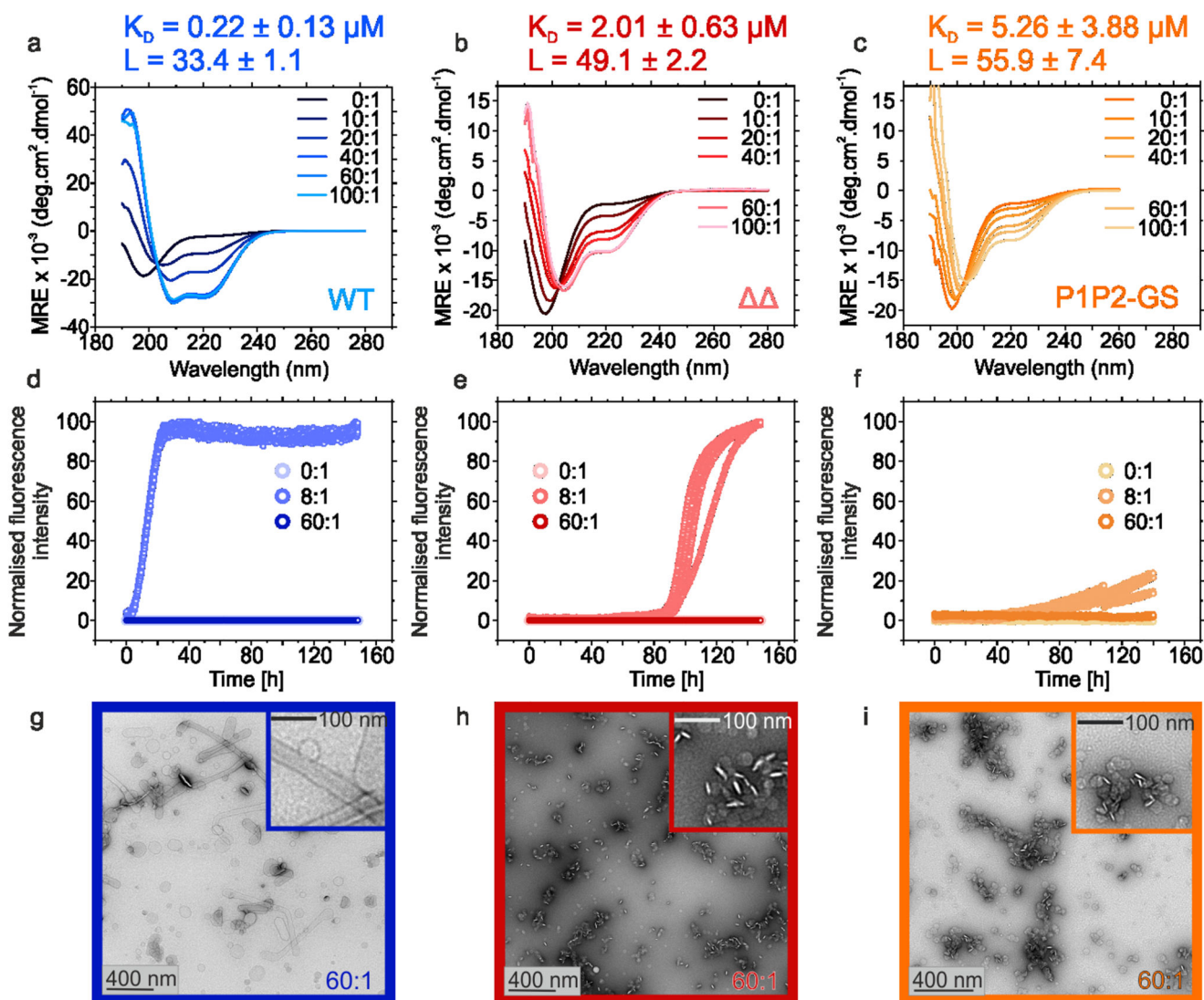


**Figure 7. Lipid-induced aggregation kinetics of WT  $\alpha$ Syn and its variants.**

a-c Far-UV CD spectra of 25  $\mu$ M WT  $\alpha$ Syn (a), (b) or P1P2-GS (c) incubated with increasing ratios of [DMPS]:[protein].  $K_D$  and L values were calculated from the change in MRE at  $\lambda_{222\text{nm}}$  fitted to a single step binding model<sup>61</sup> (Extended Data Figure 7b). Aggregation kinetics of 50  $\mu$ M  $\alpha$ Syn WT (d), (e) or P1P2-GS (f) incubated with 0:1, 8:1 or 60:1 [DMPS]:[protein] (20 mM sodium phosphate, pH 6.5; 30 °C, no shaking). g-j TEM images of representative samples of WT  $\alpha$ Syn (g), (h) or P1P2-GS (i) at the endpoint of the incubations (150 h) in the presence of 60:1 [DMPS]:[protein]. Data for graphs in a-f are available as Source Data.

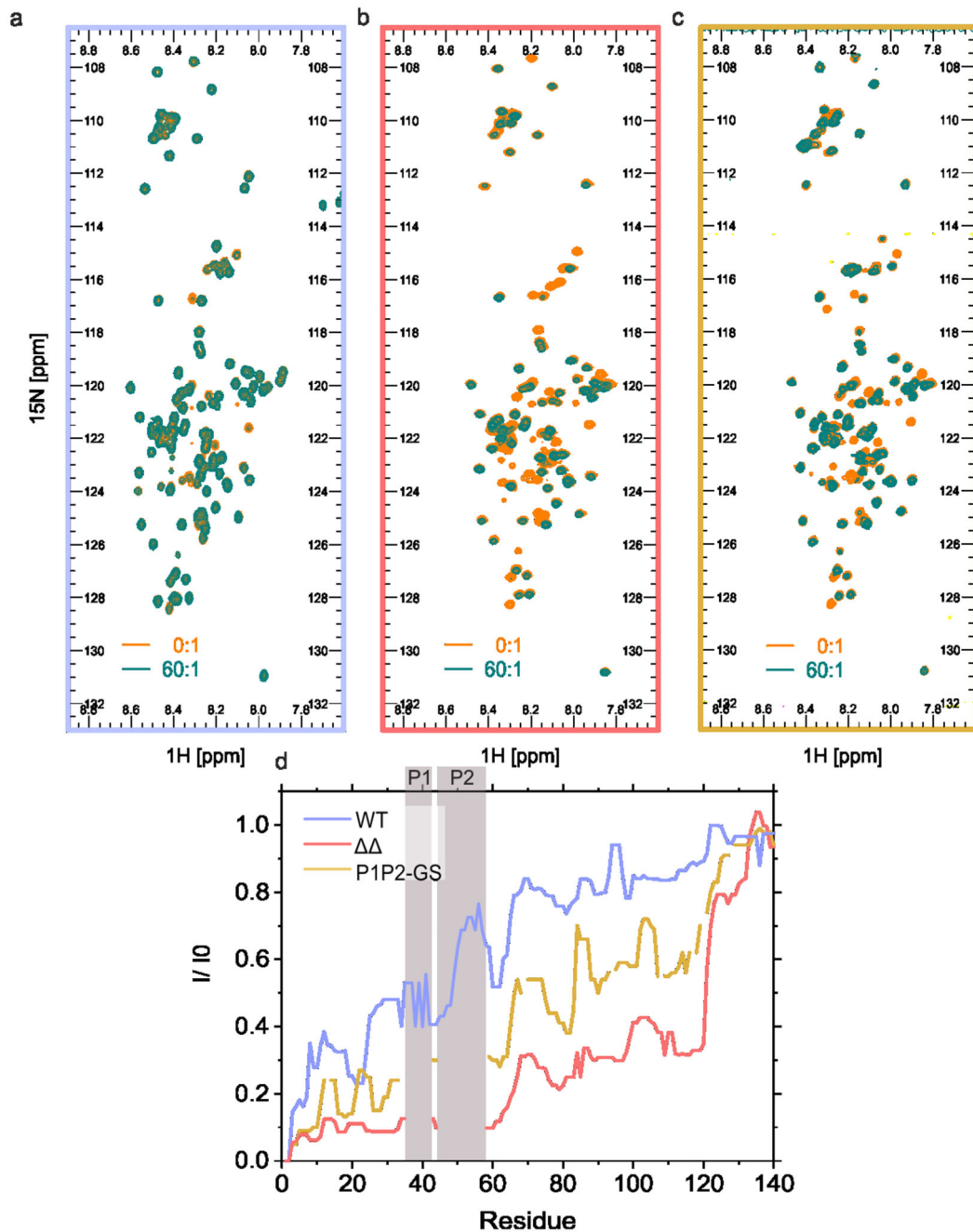


**Figure 8. NMR experiments detailing the molecular basis of liposome binding of WT  $\alpha$ Syn and P1P2-GS.**

$^1\text{H}$ - $^{15}\text{N}$  HSQC NMR spectra of a) WT  $\alpha$ Syn, b)  $\Delta\Delta$  and c) P1P2-GS in the presence (green) or absence (orange) of a 60:1 ratio of [DMPS]:[protein]. d) Intensity ratios (presence/absence of liposomes) of cross-peaks for WT  $\alpha$ Syn (blue),  $\Delta\Delta$  (red) and P1P2-GS (orange) are shown by illustrating the median value over a rolling window of five residues determined using OriginPro. The position of P1 and P2 is highlighted with grey bars. Note that residues 36-42 and 45-57 are deleted in  $\Delta\Delta$  and these residues (replaced with (SG)<sub>3</sub>S (P1) and

(GS)<sub>6</sub>G (P2)) could not be assigned for P1P2-GS. Data for graph in d are available as Source Data.